A reduced modal subspace approach for damped stochastic dynamic systems

S. Kasinos[a,b], A. Palmeri[b,*], M. Lombardo[b] and S. Adhikari[c]

[a]*Department of Aeronautics, Imperial College London, SW7 2AZ, UK*
[b]*School of Architecture, Building and Civil Engineering, Loughborough University, Loughborough, LE11 3TU, UK*
[c]*Zienkiewicz Centre for Computational Engineering, College of Engineering, Swansea University, Swansea, SA1 8EN, UK*

ARTICLE INFO

Keywords:
high-order perturbation
modal analysis
polynomial chaos expansion
random vibration
stochastic finite element method
uncertainty quantification

ABSTRACT

A novel method for characterising and propagating system uncertainty in structures subjected to dynamic actions is proposed, whereby modal shapes, frequencies and damping ratios constitute the random quantities. The latter, defined in the modal subspace rather than the full geometrical space, reduce the number of the random variables and the size of the dynamic problem. A numerical procedure is presented for their identification by calibrating their probabilistic definition in line with the geometrical space. A high-order perturbation technique is proposed for the multi-fidelity response quantification by means of an *ad hoc* extension of the conventional perturbation method. The approach involves a set of auxiliary deterministic differential equations to be adaptively solved with the piecewise exact method, and moment-cumulant relationships are employed to approximate high-order moments. Finally, a polynomial chaos expansion approach is adopted to complement the second-moment analysis for spectral quantification with the modal subspace reduction. Demonstrated on a multi-storey steel frame with semi-rigid connections and a simply supported bridge subjected to a moving load, the proposed variants exhibit improved performance with respect to the conventional second-order and improved perturbation, as well as increased flexibility, enabling the analyst to decide, on-demand, the level of fidelity, balancing accuracy and computational effort.

1. Introduction

The dynamic response of a structure subjected to earthquakes, winds and ocean waves strongly depends on the mechanical properties of the load resisting systems. Uncertainties arise when modelling the geometry, material and boundary conditions of the structure, inducing random variations in the dynamic response. Rational treatment of these uncertainties cannot be rigorously addressed when following a conventional deterministic approach. Therefore, stochastic analysis methods use knowledge of the input random variables to characterise the probabilistic structure of the response, often through first and second-order statistics, so to mitigate the unavoidable increase in computational effort.

Relevant contributions in the technical literature involve a number of analytical methods for linear structures subjected to static loads (e.g. [1–3]). For practical engineering applications, however, recourse to a finite element (FE) model is often required. Non-probabilistic uncertainty models in the context of FE analysis include the Interval FE method and the Fuzzy FE method that describe the uncertain parameters as interval variables and fuzzy sets, respectively, and therefore do not require complete probabilistic characterisation [4]. The stochastic finite element method (SFEM) [5, 6] is currently the most powerful probabilistic tool for the solution of static and dynamic problems involving FEs with random properties. Monte Carlo simulation (MCS) [7] is the simplest and most versatile variant, where a deterministic problem is repetitively solved and the response variability is characterised statistically. However, as the number of degrees-of-freedom (DoFs) and random variables increases, the computational effort may become prohibitively expensive. For this reason, alternative SFEM approaches have emerged, including the perturbation approach [8], which is based on a Taylor series expansion of the stochastic FE matrices and of the response vector, and the spectral stochastic FE method, where the model is cast in a finite dimensional setting through the Karhunen-Loève expansion [9], and the solution process is based on a spectral representation in terms of polynomial chaos (PC) decomposition [10].

*Corresponding author
a.palmeri@lboro.ac.uk (A. Palmeri)
ORCID(s): 0000-0003-0683-3436 (S. Kasinos); 0000-0001-8453-6619 (A. Palmeri); 0000-0003-0617-299X (M. Lombardo); 0000-0003-4181-3457 (S. Adhikari)

Perturbation-based approaches are computationally the least expensive methods [11], and have thus gained considerable interest over the years. A generalised stochastic perturbation technique has been applied for solving a linear elastostatic problem with a single input random variable [12]. A second-order approach has been adopted in [13] for a dynamic problem, leading to satisfactory results for small uncertainty levels of the input stochastic field. An 'improved' first-order perturbation approach that uses second-order information for the solution of static [14] and dynamic [15] problems has been found to be more accurate than the conventional second-order perturbation. Falsone and Impollonia [16] have proposed an *ad hoc* expansion of the displacement response with respect to the basic random variables for the linear static analysis of structures, capable of maintaining high level of accuracy at considerable input uncertainty levels. The method has been generalised to the geometrically nonlinear static [17] and linear dynamic [18] analyses. A frequency adaptive basis function approach was developed [19] for steady-state dynamic response of linear systems. A Neumann expansion based approach was proposed [20] for transient response analysis of structural dynamic systems with parametric uncertainty. Hua et al. [21] have used an improved first-order perturbation method for the statistical identification of FE model parameters by using measured modal parameters with randomness. More recently, a high-oder perturbation-based stochastic isogeometric method has been proposed for quantifying geometric uncertainty in shell structures [22]. The main drawback of the vast majority of the existing perturbative approaches is that they are "intrusive"; in other words, they rely on the particularisation and solution of the governing differential equations. Furthermore, they are hindered by decaying accuracy for relatively long integration times and they tend to work well for limited cases, with loss of accuracy when the level of system uncertainty increases. Finally, their suitability to accurately estimate up-to second-order statistics of the response often limits their applicability to Gaussian fields, which is scarcely the case. In fact, the response can be strongly non-Gaussian, even for linear systems, owing to the nonlinear relationship between the dynamic response and the underlying input random variables.

PC expansions provide a functional approximation of the underlying system response by means of a spectral representation on a suitably constructed basis of orth-onormal polynomial functions. Noteworthy intrusive PC approaches include Galerkin-based methods [23], such as the investigations of Jacquelin et al., who highlighted issues with the PC for the dynamic response around resonant frequencies [24] and proposed an extended Padé approach [25]. The authors recently extended their investigations on the time-domain analysis of damped stochastic linear multi-degree-of-freedom (MDoF) systems [26]. By contrast, "non-intrusive" PC schemes do not require prior knowledge of the governing differential equations. The model is treated as a black-box function and the aim is to obtain an approximation by means of a reduced set of well-chosen evaluation calls. Well-known approaches in this category include the stochastic collocation method based on Lagrange interpolation of the model response [27], projection-based approaches where the PC coefficients are cast as a multi-dimensional integral evaluated by simulation or quadrature procedures [28], and regression-based least-square minimisation techniques [29]. Blatman et al. [30] proposed an adaptive sparse PC approach based on the least angle regression algorithm. Mai et al [31]. extended the approach and proposed a stochastic time warping sparse PC for oscillatory systems. It has long been recognised that, regardless of the method used, either intrusive or non-intrusive, PC fail to represent long-term time-dependent system responses owing to their inherent increasing complexity [31]; furthermore, the required number of model evaluations increases with the size of the truncated expansion, which in turn grows with the total polynomial degree retained and the number of random variables. The overall computational burden becomes prohibitive as the number of DoFs of the spatial discretisation increases.

In this paper, the analysis of linear MDoF dynamical systems with uncertain mechanical parameters under deterministic excitation is addressed. An alternative formulation is presented, substantiated by some preliminary investigations in [32–34], where uncertainty is characterised in the reduced modal subspace, with modal shapes, modal frequencies and modal damping ratios comprising the random quantities, thus drastically reducing the number of uncertain parameters and the size of the dynamic problem. An identification procedure is presented for calibrating the probabilistic definition of the proposed uncertainty model consistently with the geometrical space. Conventional second-order and improved perturbation variants are developed in line with this model, and a novel high-order perturbation approach is proposed for the multi-fidelity quantification of the evolutionary stochastic response through and an *ad hoc* extension of the conventional perturbation approach. The proposed method involves a set of auxiliary deterministic differential equations, to be solved with the piecewise exact method (PEM), and high-order moments arising are approximated with lower ones through moment-cumulant relationships. Finally, a regression-based PC expansion is employed, complementing the second-moment analysis for spectral quantification with the modal subspace reduction. The performance of the proposed variants is compared on the seismic analysis of a pulse-driven steel frame with semi-rigid connections and a simply supported beam subjected to a moving load.

The paper is organised as follows: Section 2 briefly reviews existing perturbative methods, as formulated in the geometrical space. Section 3 presents the uncertainty model formulated in the reduced modal subspace, along with the numerical procedure for the identification of the underlying model parameters. Section 4 details the second-order and improved perturbation variants, as well as the high-order perturbation approach proposed. Section 5 addresses the spectral quantification with PC expansions. The proposed methods are numerically assessed in Section 6, and a summary of the results and findings is presented in Section 7.

2. Uncertainty in the geometric space

Let us consider a linear dynamical system ruled by the following set of second-order differential equations, conveniently arranged in a matrix form:

$$\mathbf{M}(\boldsymbol{\alpha})\,\ddot{\mathbf{u}}(t) + \mathbf{C}(\boldsymbol{\alpha})\,\dot{\mathbf{u}}(t) + \mathbf{K}(\boldsymbol{\alpha})\,\mathbf{u}(t) = \mathbf{f}(t)\,; \quad \mathbf{u}(0) = \mathbf{u}_0\,; \quad \dot{\mathbf{u}}(0) = \dot{\mathbf{u}}_0\,, \tag{1}$$

where $\mathbf{u}(t) = \left\{u_1(t) \dots u_n(t)\right\}^\top$ is the array collecting its n degrees of freedom (DoFs); $\mathbf{f}(t)$ is the vector of the applied forces; the over-dot means time derivative, and $\mathbf{u}_0$ and $\dot{\mathbf{u}}_0$ are the vectors of the initial displacements and velocities, respectively. Furthermore, $\mathbf{M}$, $\mathbf{K}$ and $\mathbf{C}$ are random matrices of mass, elastic stiffness and viscous damping, respectively, representing the only source of uncertainty of the dynamical system and, without lack of generality, they are expressed herein as functions of the vector $\boldsymbol{\alpha} = \left\{\alpha_1, \alpha_2, \dots, \alpha_N\right\}^\top$, listing N zero-mean, $\mathbb{E}\left[\alpha_i\right] = 0$, uncorrelated, $\mathbb{E}\left[\alpha_i^r \alpha_j^s\right] = \mathbb{E}\left[\alpha_i^r\right]\mathbb{E}\left[\alpha_j^s\right]$ random variables (with $i \neq j$ and $\forall r, s$), satisfying the condition $\mathbb{E}\left[\alpha_i^2\right] \ll 1$, $\mathbb{E}[\cdot]$ denoting stochastic averaging operator. It is worth mentioning here that the use of uncorrelated random variables is not unduly restrictive as it is always possible to express correlated random variables as functions of uncorrelated ones [35]. It is further noted that $\mathbf{M}$, $\mathbf{K}$ and $\mathbf{C}$ are not necessarily affected by the same subsets of random variables α_i.

2.1. Conventional second-order perturbation

Following the formulation in Ref. [15], the second-order perturbation approach is applied to Eq. (1), in the geometrical space, by imposing Taylor series expansion on $\mathbf{M}$, $\mathbf{K}$ and $\mathbf{C}$:

$$\begin{aligned}
\mathbf{M}(\boldsymbol{\alpha}) &\cong \mathbf{M}_0 + \mathbf{M}_i\alpha_i + \mathbf{M}_{i,j}\alpha_i\alpha_j\,;\\
\mathbf{K}(\boldsymbol{\alpha}) &\cong \mathbf{K}_0 + \mathbf{K}_i\alpha_i + \mathbf{K}_{i,j}\alpha_i\alpha_j\,;\\
\mathbf{C}(\boldsymbol{\alpha}) &\cong \mathbf{C}_0 + \mathbf{C}_i\alpha_i + \mathbf{C}_{i,j}\alpha_i\alpha_j\,,
\end{aligned} \tag{2}$$

where index notation is used, defined as:

$$\begin{aligned}
\mathbf{g}_0 &= \mathbf{g}(\boldsymbol{\alpha})\Big|_{\boldsymbol{\alpha}=\mathbf{0}}\,;\\
\mathbf{g}_i &= \frac{\partial \mathbf{g}(\boldsymbol{\alpha})}{\partial \alpha_i}\Big|_{\boldsymbol{\alpha}=\mathbf{0}}\,;\\
\mathbf{g}_{i,j} &= \frac{1}{2}\frac{\partial^2 \mathbf{g}(\boldsymbol{\alpha})}{\partial \alpha_i \partial \alpha_j}\Big|_{\boldsymbol{\alpha}=\mathbf{0}}\,,
\end{aligned} \tag{3}$$

and where summation is implied, here and henceforth, for the subscripted indices. Furthermore, $\mathbf{M}_0$, $\mathbf{K}_0$ and $\mathbf{C}_0$ are the matrices of mass, stiffness and damping without fluctuations, i.e. the matrices associated with the deterministic model of the structure.

The dimensions of the dynamic problem may be reduced by projecting the equations of motion onto a reduced modal subspace. Accordingly, a solution to the real-valued eigenproblem:

$$\mathbf{K}_0\,\boldsymbol{\Phi}_0 = \mathbf{M}_0\,\boldsymbol{\Phi}_0\,\boldsymbol{\Omega}_0^2 \tag{4}$$

can be sought, where $\boldsymbol{\Phi}_0 = [\boldsymbol{\phi}_1, \dots, \boldsymbol{\phi}_m]$ is the $(n \times m)$ deterministic modal matrix, normalised with respect to $\mathbf{M}_0$, whose columns are the m modal shapes, and $\boldsymbol{\Omega}_0 = \mathrm{diag}\{\omega_1, \dots, \omega_m\}$ is the deterministic diagonal spectral matrix, listing the associated modal circular frequencies.

The following transformation is then adopted:

$$\mathbf{u}(t) = \boldsymbol{\Phi}_0 \, \mathbf{q}(t) \,, \tag{5}$$

where $\mathbf{q}(t)$ is the array collecting the m modal coordinates of the structure which are retained in the analysis, and in general $m \ll n$.

Upon substitution of Eq. (5) in Eq. (1), premultiplication of the result by $\boldsymbol{\Phi}_0^{\top}$, and further manipulations, one obtains:

$$\mathbf{m}\,(\boldsymbol{\alpha})\,\ddot{\mathbf{q}}(t) + \boldsymbol{\Xi}\,(\boldsymbol{\alpha})\,\dot{\mathbf{q}}(t) + \boldsymbol{\Omega}^2\,(\boldsymbol{\alpha})\,\mathbf{q}(t) = \mathbf{F}(t) \,, \tag{6}$$

where the explicit dependency of the vectors $\mathbf{q}(t) = \mathbf{q}(t, \boldsymbol{\alpha})$, $\dot{\mathbf{q}}(t) = \dot{\mathbf{q}}(t, \boldsymbol{\alpha})$ and $\ddot{\mathbf{q}}(t) = \ddot{\mathbf{q}}(t, \boldsymbol{\alpha})$ on the vector of random variables $\boldsymbol{\alpha}$ has been omitted for the sake of simplifying the notation, and where the vectors of initial conditions and external forces are given by:

$$\mathbf{q}(0) = \boldsymbol{\Phi}_0^{\top} \, \mathbf{M}_0 \, \mathbf{u}_0 \,; \quad \dot{\mathbf{q}}(0) = \boldsymbol{\Phi}_0^{\top} \, \mathbf{M}_0 \, \dot{\mathbf{u}}_0 \,; \quad \mathbf{F}(t) = \boldsymbol{\Phi}_0^{\top} \, \mathbf{f}(t) \,, \tag{7}$$

the superscripted $\top$ being the transpose operator; furthermore, the matrices $\mathbf{m}$, $\boldsymbol{\Omega}^2$ and $\boldsymbol{\Xi}$ are defined as:

$$\begin{aligned}
\mathbf{m}\,(\boldsymbol{\alpha}) &= \mathbf{I}_m + \mathbf{m}_i \alpha_i + \mathbf{m}_{i,j} \alpha_i \alpha_j \,; \\
\boldsymbol{\Omega}^2\,(\boldsymbol{\alpha}) &= \boldsymbol{\Omega}_0^2 + \boldsymbol{\Omega}_i^2 \alpha_i + \boldsymbol{\Omega}_{i,j}^2 \alpha_i \alpha_j \,; \\
\boldsymbol{\Xi}\,(\boldsymbol{\alpha}) &= \boldsymbol{\Xi}_0 + \boldsymbol{\Xi}_i \alpha_i + \boldsymbol{\Xi}_{i,j} \alpha_i \alpha_j \,.
\end{aligned} \tag{8}$$

and play the role of the matrices of mass, stiffness and damping in the reduced modal subspace, respectively, with the following relationships arising:

$$\begin{aligned}
&\mathbf{I}_m = \boldsymbol{\Phi}_0^{\top} \mathbf{M}_0 \boldsymbol{\Phi}_0 \,; \quad \mathbf{m}_i = \boldsymbol{\Phi}_0^{\top} \mathbf{M}_i \boldsymbol{\Phi}_0 \,; \quad \mathbf{m}_{i,j} = \boldsymbol{\Phi}_0^{\top} \mathbf{M}_{i,j} \boldsymbol{\Phi}_0 \,; \\
&\boldsymbol{\Omega}_0^2 = \boldsymbol{\Phi}_0^{\top} \mathbf{K}_0 \boldsymbol{\Phi}_0 \,; \quad \boldsymbol{\Omega}_i^2 = \boldsymbol{\Phi}_0^{\top} \mathbf{K}_i \boldsymbol{\Phi}_0 \,; \quad \boldsymbol{\Omega}_{i,j}^2 = \boldsymbol{\Phi}_0^{\top} \mathbf{K}_{i,j} \boldsymbol{\Phi}_0 \,; \\
&\boldsymbol{\Xi}_0 = \boldsymbol{\Phi}_0^{\top} \mathbf{C}_0 \boldsymbol{\Phi}_0 \,; \quad \boldsymbol{\Xi}_i = \boldsymbol{\Phi}_0^{\top} \mathbf{C}_i \boldsymbol{\Phi}_0 \,; \quad \boldsymbol{\Xi}_{i,j} = \boldsymbol{\Phi}_0^{\top} \mathbf{C}_{i,j} \boldsymbol{\Phi}_0 \,,
\end{aligned} \tag{9}$$

in which $\mathbf{I}_m$ is the identity matrix of size m. It should be noted that, while $\boldsymbol{\Omega}_0^2 = \left[\boldsymbol{\Omega}_0\right]^2$ is the actual second-power matrix of the deterministic spectral matrix $\boldsymbol{\Omega}_0$ (so it is positive definite), the matrices $\boldsymbol{\Omega}_i^2$ and $\boldsymbol{\Omega}_{i,j}^2$ collect the derivatives of the squared modal frequencies $\omega_1^2, \ldots, \omega_m^2$ with respect to the random variables α_i and α_j, meaning that in general $\boldsymbol{\Omega}_i^2 = 2\,\boldsymbol{\Omega}_0\,\boldsymbol{\Omega}_i \neq \left[\boldsymbol{\Omega}_i\right]^2$, $\boldsymbol{\Omega}_{i,j}^2 = 2\left[\boldsymbol{\Omega}_i\,\boldsymbol{\Omega}_j + \boldsymbol{\Omega}_0\,\boldsymbol{\Omega}_{i,j}\right] \neq \left[\boldsymbol{\Omega}_{i,j}\right]^2$ and they are not necessarily positive definite.

Eq. (6) is cast in state-space form:

$$\dot{\mathbf{z}}(t, \boldsymbol{\alpha}) = \mathbf{D}(\boldsymbol{\alpha})\,\mathbf{z}(t, \boldsymbol{\alpha}) + \mathbf{V}(\boldsymbol{\alpha})\,\mathbf{F}(t) \,, \tag{10}$$

where $\mathbf{z}(t, \boldsymbol{\alpha})$ is the response state vector and $\mathbf{D}(\boldsymbol{\alpha})$ is the dynamic matrix, given by:

$$\begin{aligned}
\mathbf{z}(t, \boldsymbol{\alpha}) &= \begin{Bmatrix} \mathbf{q}(t) \\ \dot{\mathbf{q}}(t) \end{Bmatrix} \,; \quad \mathbf{z}(0, \boldsymbol{\alpha}) = \begin{Bmatrix} \mathbf{q}_0 \\ \dot{\mathbf{q}}_0 \end{Bmatrix} \,; \\
\mathbf{D}(\boldsymbol{\alpha}) &= \begin{bmatrix} \mathbf{O}_{m \times m} & \mathbf{I}_m \\ -\mathbf{m}^{-1}(\boldsymbol{\alpha})\,\boldsymbol{\Omega}^2(\boldsymbol{\alpha}) & -\mathbf{m}^{-1}(\boldsymbol{\alpha})\,\boldsymbol{\Xi}(\boldsymbol{\alpha}) \end{bmatrix} \,; \\
\mathbf{V}(\boldsymbol{\alpha}) &= \begin{bmatrix} \mathbf{O}_{m \times m} \\ \mathbf{m}^{-1}(\boldsymbol{\alpha}) \end{bmatrix} \,,
\end{aligned} \tag{11}$$

in which the symbol $\mathbf{O}_{r \times s}$ defines a zero matrix with r rows and s columns.

Series expansion of Eq. (11) gives:

$$\begin{aligned}
\mathbf{z}(t,\boldsymbol{\alpha}) &\cong \mathbf{z}_0(t) + \mathbf{z}_i(t)\,\alpha_i + \mathbf{z}_{i,j}(t)\,\alpha_i\,\alpha_j\,; \\
\mathbf{D}(\boldsymbol{\alpha}) &\cong \mathbf{D}_0 + \mathbf{D}_i\,\alpha_i + \mathbf{D}_{i,j}\,\alpha_i\,\alpha_j\,; \\
\mathbf{V}(\boldsymbol{\alpha}) &\cong \mathbf{V}_0 + \mathbf{V}_i\,\alpha_i + \mathbf{V}_{i,j}\,\alpha_i\,\alpha_j\,,
\end{aligned} \tag{12}$$

where $\mathbf{z}_i(t)$ and $\mathbf{z}_{i,j}(t)$ play the role of first-order and second-order sensitivity vectors of the state-space dynamic response of the structure in the reduce modal space, and where the dynamic matrices $\mathbf{D}_0$, $\mathbf{D}_i$ and $\mathbf{D}_{i,j}$ and the load vectors $\mathbf{V}_0$, $\mathbf{V}_i$ and $\mathbf{V}_{i,j}$ are provided in Ref. [15].

In expanding $\mathbf{m}^{-1}(\boldsymbol{\alpha})$, partial derivatives are obtained by the use of the rule for inverse matrix differentiation [36], as detailed in Appendix A.1.

Importantly, the quantities appearing in the series expansion of $\mathbf{z}(t,\boldsymbol{\alpha})$ can be expressed as a solution of the following set of $1 + N + N^2$ deterministic equations governing the uncertainty propagation (UP):

$$\dot{\mathbf{z}}_0 = \mathbf{D}_0\mathbf{z}_0 + \mathbf{V}_0\mathbf{F}(t)\,; \tag{13a}$$

$$\dot{\mathbf{z}}_i = \mathbf{D}_0\mathbf{z}_i + \mathbf{D}_i\mathbf{z}_0 + \mathbf{V}_i\mathbf{F}(t)\,,\ \ i = 1,\dots,N\,; \tag{13b}$$

$$\dot{\mathbf{z}}_{i,j} = \mathbf{D}_0\mathbf{z}_{i,j} + \mathbf{D}_i\mathbf{z}_j + \mathbf{D}_{i,j}\mathbf{z}_0 + \mathbf{V}_{i,j}\mathbf{F}(t)\,,\ \ i,j = 1,\dots,N\,, \tag{13c}$$

in which, to simplify the notation, the time-dependency of the $(2\,m \times 1)$ vectors $\mathbf{z}_0 = \mathbf{z}_0(t)$, $\mathbf{z}_i = \mathbf{z}_i(t)$ and $\mathbf{z}_{i,j} = \mathbf{z}_{i,j}(t)$ has not been shown explicitely.

The time-varying second-order statistics of the response in terms of mean values and variances are finally obtained as:

$$\begin{aligned}
&\mathbb{E}\left[\mathbf{z}(t)\right] = \mathbf{z}_0 + \mathbf{z}_{i,j}\,\mathbb{E}[\alpha_i\alpha_j] = \mathbf{z}_0 + \mathbf{z}_{i,i}\,\mathbb{E}[\alpha_i^2]\,; \\
&\mathrm{Var}\left[\mathbf{z}(t)\right] = \mathbb{E}\left[\left(\mathbf{z}(t)\odot\mathbf{z}(t)\right)\right] - \left(\mathbb{E}\left[\mathbf{z}(t)\right]\odot\mathbb{E}\left[\mathbf{z}(t)\right]\right) = \\
&\qquad = \left(\mathbf{z}_i\odot\mathbf{z}_j\right)\,\mathbb{E}[\alpha_i\alpha_j] - \left(\mathbf{z}_{i,j}\odot\mathbf{z}_{k,l}\right)\,\mathbb{E}[\alpha_i\alpha_j]\mathbb{E}[\alpha_k\alpha_l] \\
&\qquad\quad + \left\{\left(\mathbf{z}_i\odot\mathbf{z}_{j,k}\right) + \left(\mathbf{z}_{i,j}\odot\mathbf{z}_k\right)\right\}\,\mathbb{E}[\alpha_i\alpha_j\alpha_k] + \left(\mathbf{z}_{i,j}\odot\mathbf{z}_{k,l}\right)\,\mathbb{E}[\alpha_i\alpha_j\alpha_k\alpha_l]\ .
\end{aligned} \tag{14}$$

where the notation $\left(\mathbf{z}\odot\mathbf{z}\right)$ denotes the element-wise product, also known as Hadamard multiplication (e.g. Ref. [37]).

It is emphasised here that statistical moments of the random variables α_i up to the the fourth order are required to calculate the variance of the dynamic response of the structure; if only the first two statistical moments are available for the random variables α_i, then only the first term could be retained in the first of Eqs. (12), leading to the following simplified expression:

$$\mathrm{Var}\left[\mathbf{z}(t)\right] \cong \left(\mathbf{z}_i\odot\mathbf{z}_j\right)\,\mathbb{E}[\alpha_i\alpha_j] = \left(\mathbf{z}_i\odot\mathbf{z}_i\right)\,\mathbb{E}[\alpha_i^2]\ . \tag{15}$$

2.2. Improved perturbation

As an alternative to the conventional perturbation approach, the so-called improved perturbation approach can be adopted, as suggested for instance in Refs. [14, 15].

Stochastic averaging of Eq. (2) gives:

$$\begin{aligned}
\bar{\mathbf{M}} &= \mathbf{M}_0 + \mathbf{M}_{i,i}\,\mathbb{E}[\alpha_i^2]\,; \\
\bar{\mathbf{K}} &= \mathbf{K}_0 + \mathbf{K}_{i,i}\,\mathbb{E}[\alpha_i^2]\,; \\
\bar{\mathbf{C}} &= \mathbf{C}_0 + \mathbf{C}_{i,i}\,\mathbb{E}[\alpha_i^2]\,,
\end{aligned} \tag{16}$$

where the upper bar denotes mean value, which in general differs from the respective deterministic value, designated with the subscripted zero.

Neglecting second-order terms in Eq. (2), substitution of Eq. (16) gives:

$$\begin{aligned}\mathbf{M}(\boldsymbol{\alpha}) &\cong \bar{\mathbf{M}} + \delta\mathbf{M}(\boldsymbol{\alpha}) \;;\\ \mathbf{K}(\boldsymbol{\alpha}) &\cong \bar{\mathbf{K}} + \delta\mathbf{K}(\boldsymbol{\alpha}) \;;\\ \mathbf{C}(\boldsymbol{\alpha}) &\cong \bar{\mathbf{C}} + \delta\mathbf{C}(\boldsymbol{\alpha}) \;,\end{aligned} \tag{17}$$

where δ denotes deviation from the mean, given by:

$$\begin{aligned}\delta\mathbf{M}(\boldsymbol{\alpha}) &= \mathbf{M}_i\,\alpha_i \;;\\ \delta\mathbf{K}(\boldsymbol{\alpha}) &= \mathbf{K}_i\,\alpha_i \;;\\ \delta\mathbf{C}(\boldsymbol{\alpha}) &= \mathbf{C}_i\,\alpha_i \;.\end{aligned} \tag{18}$$

The following modal coordinate transformation is used (similar to Eq. (5)):

$$\mathbf{u}(t) = \bar{\boldsymbol{\Phi}}\,\mathbf{q}(t)\,, \tag{19}$$

where the modal matrix $\bar{\boldsymbol{\Phi}}$, normalised with respect to $\bar{\mathbf{M}}$, satisfies the real-valued eigenproblem (similar to Eq. (4)):

$$\bar{\mathbf{K}}\,\bar{\boldsymbol{\Phi}} = \bar{\mathbf{M}}\,\bar{\boldsymbol{\Phi}}\,\bar{\boldsymbol{\Omega}}^2 \tag{20}$$

involving the mean values of mass and stiffness matrix, and $\bar{\boldsymbol{\Omega}}$ is the associated spectral matrix. Importantly, in general, $\mathbb{E}[\boldsymbol{\Phi}(\boldsymbol{\alpha})] \neq \bar{\boldsymbol{\Phi}} \neq \boldsymbol{\Phi}_0$ and $\mathbb{E}[\boldsymbol{\Omega}(\boldsymbol{\alpha})] \neq \bar{\boldsymbol{\Omega}} \neq \boldsymbol{\Omega}_0$.

Upon further manipulations, the equation of motion in the reduced modal subspace retains the form of Eq. (6), with the following vectors of initial conditions and dynamic loads (similar to Eqs. (7)):

$$\mathbf{q}(0) = \bar{\boldsymbol{\Phi}}^{\top}\bar{\mathbf{M}}\,\mathbf{u}_0 \;;\quad \dot{\mathbf{q}}(0) = \bar{\boldsymbol{\Phi}}^{\top}\bar{\mathbf{M}}\,\dot{\mathbf{u}}_0 \;;\quad \bar{\mathbf{F}}(t) = \bar{\boldsymbol{\Phi}}^{\top}\mathbf{f}(t)\,. \tag{21}$$

The following relationships then arise:

$$\begin{aligned}\mathbf{m}(\boldsymbol{\alpha}) &= \mathbf{I}_m + \bar{\mathbf{m}}_i\alpha_i \;;\\ \boldsymbol{\Omega}^2(\boldsymbol{\alpha}) &= \bar{\boldsymbol{\Omega}}^2 + \bar{\boldsymbol{\Omega}}_i^2\alpha_i \;;\\ \boldsymbol{\Xi}(\boldsymbol{\alpha}) &= \bar{\boldsymbol{\Xi}} + \bar{\boldsymbol{\Xi}}_i\alpha_i \;,\end{aligned} \tag{22}$$

where:

$$\begin{aligned}\mathbf{I}_m &= \bar{\boldsymbol{\Phi}}^{\top}\bar{\mathbf{M}}\,\bar{\boldsymbol{\Phi}} \;;\quad \bar{\mathbf{m}}_i = \bar{\boldsymbol{\Phi}}^{\top}\mathbf{M}_i\,\bar{\boldsymbol{\Phi}} \;;\\ \bar{\boldsymbol{\Omega}}^2 &= \bar{\boldsymbol{\Phi}}^{\top}\bar{\mathbf{K}}\,\bar{\boldsymbol{\Phi}} \;;\quad \bar{\boldsymbol{\Omega}}_i^2 = \bar{\boldsymbol{\Phi}}^{\top}\mathbf{K}_i\,\bar{\boldsymbol{\Phi}} \;;\\ \bar{\boldsymbol{\Xi}} &= \bar{\boldsymbol{\Phi}}^{\top}\bar{\mathbf{C}}\,\bar{\boldsymbol{\Phi}} \;;\quad \bar{\boldsymbol{\Xi}}_i = \bar{\boldsymbol{\Phi}}^{\top}\mathbf{C}_i\,\bar{\boldsymbol{\Phi}} \;.\end{aligned} \tag{23}$$

Importantly, even if the same notation has been used for the vectors of modal coordinates $\mathbf{q}(t)$ and modal excitations $\mathbf{F}(t)$ in presenting the conventional and improved perturbation approaches, these quantities are in fact different as they are associated with different pairs of eigenvectors and eigenvalues; namely, $\{\boldsymbol{\Phi}_0, \boldsymbol{\Omega}_0\}$ for the conventional perturbation and $\{\bar{\boldsymbol{\Phi}}, \bar{\boldsymbol{\Omega}}\}$ for the improved perturbation.

Eq. (10) still holds here, where the improved perturbation approach procedure is successively employed on the expanded underlying quantities, giving rise to:

$$\begin{aligned}\mathbf{z}(t,\boldsymbol{\alpha}) &\cong \bar{\mathbf{z}} + \delta\mathbf{z}(t,\boldsymbol{\alpha}) = \bar{\mathbf{z}} + \mathbf{z}_i\alpha_i \;;\\ \mathbf{D}(\boldsymbol{\alpha}) &\cong \bar{\mathbf{D}} + \delta\mathbf{D}(\boldsymbol{\alpha}) = \bar{\mathbf{D}} + \mathbf{D}_i\alpha_i \;;\\ \mathbf{V}(\boldsymbol{\alpha}) &\cong \bar{\mathbf{V}} + \delta\mathbf{V}(\boldsymbol{\alpha}) = \bar{\mathbf{V}} + \mathbf{V}_i\alpha_i \;,\end{aligned} \tag{24}$$

where the vectors $\bar{\mathbf{z}} = \bar{\mathbf{z}}(t)$ and $\mathbf{z}_i = \mathbf{z}_i(t)$ are time-dependent and the expressions for $\bar{\mathbf{D}}$, $\mathbf{D}_i$, $\bar{\mathbf{V}}$ and $\mathbf{V}_i$ can be found in

Ref. [15].

Following manipulations, a system of $1 + N$ coupled UP equations is obtained:

$$\begin{aligned} \dot{\bar{\mathbf{z}}} &= \bar{\mathbf{D}}\,\bar{\mathbf{z}} + \mathbf{D}_i\,\mathbf{z}_i\,\mathbb{E}[\alpha_i^2] + \bar{\mathbf{V}}\,\mathbf{F}(t)\,; \\ \dot{\mathbf{z}}_i &= \bar{\mathbf{D}}\,\mathbf{z}_i + \mathbf{D}_i\,\bar{\mathbf{z}} + \mathbf{V}_i\,\mathbf{F}(t)\,,\ i = 1,\dots,N\,, \end{aligned} \tag{25}$$

which can be numerically solved.

The statistics of the response are finally obtained as:

$$\begin{aligned} &\mathbb{E}\left[\mathbf{z}(t)\right] = \bar{\mathbf{z}}\,; \\ &\mathrm{Var}\left[\mathbf{z}(t)\right] = \left(\mathbf{z}_i \odot \mathbf{z}_i\right)\mathbb{E}[\alpha_i^2]\,. \end{aligned} \tag{26}$$

Notably, when compared to the conventional approach, there is an improvement in the first term of the associated quantities being expanded. This is due to the evaluation of the perturbation about an improved approximation of the mean value rather than about the deterministic one [14, 15].

3. Uncertainty in the modal space

In the previous section, the conventional and improved perturbation methods have been summarised for the analysis of linear dynamical systems. In this section, an alternative formulation is presented whereby the problem is conveniently cast in the reduced modal subspace. The proposed model defines the underlying random variables directly in terms of modal quantities. Accordingly, their number can be reduced quite drastically with respect to the geometrical space ($\mathcal{N} \ll N$) and the resulting computational burden is also reduced, thus forming the basis for the development of the high-fidelity response quantification methods detailed in subsequent sections.

3.1. Randomisation scheme

Considering random fluctuations in the modal shapes, circular frequencies and viscous damping ratios, for $m \geq 2$ modes, the following definition of the stochastic $(m \times m)$ matrices can be assumed:

$$\begin{aligned} \boldsymbol{\Phi}\left(\boldsymbol{\alpha}\right) &= \bar{\boldsymbol{\Phi}}\left(\mathbf{I}_m + \boldsymbol{\beta}\right) = \begin{bmatrix} (1+\beta_{1,1})\bar{\boldsymbol{\phi}}_1^{\top} + \beta_{2,1}\bar{\boldsymbol{\phi}}_2^{\top} + \cdots + \beta_{m,1}\bar{\boldsymbol{\phi}}_m^{\top} \\ \beta_{1,2}\bar{\boldsymbol{\phi}}_1^{\top} + (1+\beta_{2,2})\bar{\boldsymbol{\phi}}_2^{\top} + \cdots + \beta_{m,2}\bar{\boldsymbol{\phi}}_m^{\top} \\ \vdots \\ \beta_{1,m}\bar{\boldsymbol{\phi}}_1^{\top} + \beta_{2,m}\bar{\boldsymbol{\phi}}_2^{\top} + \cdots + (1+\beta_{m,m})\bar{\boldsymbol{\phi}}_m^{\top} \end{bmatrix}^{\top}; \\ \boldsymbol{\Omega}\left(\boldsymbol{\alpha}\right) &= \bar{\boldsymbol{\Omega}}\left(\mathbf{I}_m + \boldsymbol{\gamma}\right) = \mathrm{diag}\left[\bar{\omega}_i\left(1+\gamma_i\right)\right]\,; \\ \boldsymbol{\Xi}\left(\boldsymbol{\alpha}\right) &= 2\,\boldsymbol{\zeta}\left(\boldsymbol{\alpha}\right)\boldsymbol{\Omega}\left(\boldsymbol{\alpha}\right)\,;\ \boldsymbol{\zeta}\left(\boldsymbol{\alpha}\right) = \bar{\boldsymbol{\zeta}}\left(\mathbf{I}_m + \boldsymbol{\theta}\right) = \mathrm{diag}\left[\bar{\zeta}_i\left(1+\theta_i\right)\right]\,, \end{aligned} \tag{27}$$

where $\boldsymbol{\beta}$ is in general a fully populated $(m \times m)$ random matrix, in which the generic zero-mean random variable $\beta_{i,j}$ quantifies the uncertainty in the jth mode projected onto the ith mode of the 'mean structure', i.e. the structure with mean mass matrix $\bar{\mathbf{M}}$ and mean elastic stiffness $\bar{\mathbf{K}}$ (see Eq. (20)), as schematically represented in Figure 1; $\boldsymbol{\gamma}$ and $\boldsymbol{\theta}$ are diagonal random matrices of size m, where the zero-mean random variables γ_i and θ_i are associated with the ith circular frequency and viscous damping ratio, respectively; and it is further assumed that the above random variables are statistically uncorrelated, and that $|\beta_{i,j}|, |\gamma_i|, |\theta_i| \ll 1$.

According to the proposed randomisation scheme, the random vector $\boldsymbol{\alpha} = \left\{\beta_{1,1}, \beta_{1,2}, \cdots, \beta_{m,m}, \gamma_1, \cdots, \gamma_m, \theta_1 \ \cdots, \theta_m\right\}^{\top}$ concatenates the non-zero elements of $\boldsymbol{\beta}$, $\boldsymbol{\gamma}$ and $\boldsymbol{\theta}$, giving rise to a significantly reduced set of up-to

$$\mathcal{N} = m^2 + 2\,m \tag{28}$$

random variables, with $\mathcal{N} \ll N$, fully characterising the probabilistic definition of the structural system.

It is emphasised, that the random vector $\boldsymbol{\alpha}$ only contains this reduced set of random variables, and it therefore particularises the one defined in §2.

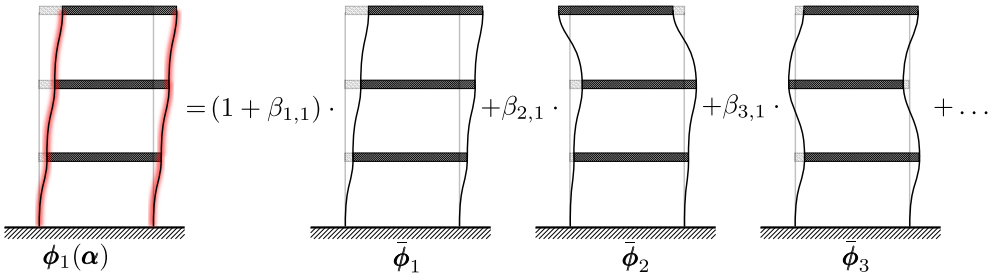

Figure 1: Uncertainty characterisation in the first mode of a simple three-storey planar frame.

3.2. Randomised mass, stiffness and damping matrices

The elements of the stochastic matrices $\boldsymbol{\beta}, \boldsymbol{\gamma}$, and $\boldsymbol{\theta}$ can either be quantified directly in the reduced modal space through experimental observations i.e. operational modal analysis, for existing structures (e.g. Refs. [38–40]), or through numerical procedures, e.g. at the design stage. In the latter case, relationships between uncertainties in the modal and geometrical spaces need to be established.

To achieve this, the random fluctuations about the mean values of the the mass, stiffness and damping matrices in the geometrical space can be conveniently expressed as (see Eqs. (17)):

$$\begin{aligned} \delta\mathbf{M}(\boldsymbol{\alpha}) &= \widetilde{\mathbf{M}}(\boldsymbol{\alpha}) - \widetilde{\mathbf{M}}\,; \\ \delta\mathbf{K}(\boldsymbol{\alpha}) &= \widetilde{\mathbf{K}}(\boldsymbol{\alpha}) - \widetilde{\mathbf{K}}\,; \\ \delta\mathbf{C}(\boldsymbol{\alpha}) &= \widetilde{\mathbf{C}}(\boldsymbol{\alpha}) - \widetilde{\mathbf{C}}\,, \end{aligned} \tag{29}$$

where the application of inverse orthogonality relations gives:

$$\begin{aligned} \widetilde{\mathbf{M}}(\boldsymbol{\alpha}) &= \bar{\mathbf{M}}\boldsymbol{\Phi}(\boldsymbol{\alpha})\boldsymbol{\Phi}^{\mathsf{T}}(\boldsymbol{\alpha})\bar{\mathbf{M}}\,; \\ \widetilde{\mathbf{K}}(\boldsymbol{\alpha}) &= \bar{\mathbf{M}}\boldsymbol{\Phi}(\boldsymbol{\alpha})\boldsymbol{\Omega}^2(\boldsymbol{\alpha})\boldsymbol{\Phi}^{\mathsf{T}}(\boldsymbol{\alpha})\bar{\mathbf{M}}\,; \\ \widetilde{\mathbf{C}}(\boldsymbol{\alpha}) &= \bar{\mathbf{M}}\boldsymbol{\Phi}(\boldsymbol{\alpha})2\boldsymbol{\zeta}(\boldsymbol{\alpha})\boldsymbol{\Omega}(\boldsymbol{\alpha})\boldsymbol{\Phi}^{\mathsf{T}}(\boldsymbol{\alpha})\bar{\mathbf{M}}\,, \end{aligned} \tag{30}$$

and:

$$\begin{aligned} \widetilde{\mathbf{M}} &= \bar{\mathbf{M}}\bar{\boldsymbol{\Phi}}\bar{\boldsymbol{\Phi}}^{\mathsf{T}}\bar{\mathbf{M}}\,; \\ \widetilde{\mathbf{K}} &= \bar{\mathbf{M}}\bar{\boldsymbol{\Phi}}\bar{\boldsymbol{\Omega}}^2\bar{\boldsymbol{\Phi}}^{\mathsf{T}}\bar{\mathbf{M}}\,; \\ \widetilde{\mathbf{C}} &= \bar{\mathbf{M}}\bar{\boldsymbol{\Phi}}2\bar{\boldsymbol{\zeta}}\bar{\boldsymbol{\Omega}}\bar{\boldsymbol{\Phi}}^{\mathsf{T}}\bar{\mathbf{M}}\,, \end{aligned} \tag{31}$$

to in which the over tilde indicates modal approximation. Importantly, the fidelity of the model increases with the number of modes retained in analysis; that is, for $m \to n$, $\widetilde{\mathbf{M}}(\boldsymbol{\alpha}) \to \mathbf{M}(\boldsymbol{\alpha})$, $\widetilde{\mathbf{K}}(\boldsymbol{\alpha}) \to \mathbf{K}(\boldsymbol{\alpha})$ and $\widetilde{\mathbf{C}}(\boldsymbol{\alpha}) \to \mathbf{C}(\boldsymbol{\alpha})$.

If the modal transformation of Eq. (19) is adopted to project the equations of motion onto the reduced modal subspace, the associated matrices of mass, stiffness and damping read:

$$\begin{aligned} \mathbf{m}(\boldsymbol{\alpha}) &= \bar{\boldsymbol{\Phi}}^{\mathsf{T}}\bar{\mathbf{M}}\boldsymbol{\Phi}(\boldsymbol{\alpha})\boldsymbol{\Phi}^{\mathsf{T}}(\boldsymbol{\alpha})\bar{\mathbf{M}}\bar{\boldsymbol{\Phi}} = \mathbf{I}_m + \delta\mathbf{m}(\boldsymbol{\alpha})\,; \\ \mathbf{k}(\boldsymbol{\alpha}) &= \bar{\boldsymbol{\Phi}}^{\mathsf{T}}\bar{\mathbf{M}}\boldsymbol{\Phi}(\boldsymbol{\alpha})\boldsymbol{\Omega}^2(\boldsymbol{\alpha})\boldsymbol{\Phi}^{\mathsf{T}}(\boldsymbol{\alpha})\bar{\mathbf{M}}\bar{\boldsymbol{\Phi}} = \bar{\boldsymbol{\Omega}}^2 + \delta\mathbf{k}(\boldsymbol{\alpha})\,; \\ \mathbf{c}(\boldsymbol{\alpha}) &= \bar{\boldsymbol{\Phi}}^{\mathsf{T}}\bar{\mathbf{M}}\boldsymbol{\Phi}(\boldsymbol{\alpha})2\boldsymbol{\zeta}(\boldsymbol{\alpha})\boldsymbol{\Omega}(\boldsymbol{\alpha})\boldsymbol{\Phi}^{\mathsf{T}}(\boldsymbol{\alpha})\bar{\mathbf{M}}\bar{\boldsymbol{\Phi}} = 2\bar{\boldsymbol{\zeta}}\bar{\boldsymbol{\Omega}} + \delta\mathbf{c}(\boldsymbol{\alpha})\,. \end{aligned} \tag{32}$$

3.3. Identification of model parameters

A simple numerical procedure is next presented for calibrating the random variables of the proposed uncertainty model, focussing on the elements of the random matrices $\boldsymbol{\beta}$ and $\boldsymbol{\gamma}$ that define the assumed random fluctuations in the real-valued eigenvectors and eigenvalues of the structure (see Eq. (27)). The purpose for this procedure is twofold. First, to develop a rational general methodology that allows taking into account random variables associated with physical

characteristics of the structure in the geometrical space. Second, to rank them in terms of their relative significance, thus enabling to retain only the dominant ones, in line with the sparsity-of-effects principle (e.g. Refs. [41, 42]).

In doing this, Eq. (27) can be rearranged, leading to the following inverse relationships, expressed in terms of the rth realisation of a MCS:

$$\hat{\boldsymbol{\beta}}^{(r)} = \boldsymbol{\Phi}_0^{\top}\,\mathbf{M}_0\,\boldsymbol{\Phi}^{(r)} - \mathbf{I}_m\,; \tag{33a}$$

$$\hat{\boldsymbol{\gamma}}^{(r)} = \boldsymbol{\Omega}_0^{-1}\,\boldsymbol{\Omega}^{(r)} - \mathbf{I}_m\,, \tag{33b}$$

where $\mathbf{K}^{(r)}\,\boldsymbol{\Phi}^{(r)} = \mathbf{M}^{(r)}\,\boldsymbol{\Phi}^{(r)}\left[\boldsymbol{\Omega}^{(r)}\right]^2$, with $\left[\boldsymbol{\Phi}^{(r)}\right]^{\top}\mathbf{M}^{(r)}\,\boldsymbol{\Phi}^{(r)} = \mathbf{I}_m$, while $\mathbf{M}_0$, $\boldsymbol{\Phi}_0$ and $\boldsymbol{\Omega}_0$ are the deterministic matrices appearing Eq. (4); furthermore, the over-hat signifies that, in general, $\mathbb{E}[\hat{\boldsymbol{\beta}}] = \bar{\boldsymbol{\beta}} \neq \mathbf{O}_{m\times m}$ and $\mathbb{E}[\hat{\boldsymbol{\gamma}}] = \bar{\boldsymbol{\gamma}} \neq \mathbf{O}_{m\times m}$. Importantly, no limiting assumptions are required in the definition of the uncertainty in the geometrical space.

Mean modal and spectral matrices can then be evaluated as:

$$\bar{\boldsymbol{\Phi}} = \boldsymbol{\Phi}_0\left[\mathbf{I}_m + \bar{\boldsymbol{\beta}}\right]\,; \tag{34a}$$

$$\bar{\boldsymbol{\Omega}} = \boldsymbol{\Omega}_0\left[\mathbf{I}_m + \bar{\boldsymbol{\gamma}}\right]\,, \tag{34b}$$

and following relationships can be used to arrive to the sought zero mean-random variables:

$$\beta_{i,j}^{(r)} = \frac{\hat{\beta}_{i,j}^{(r)} - \bar{\beta}_{i,j}}{\bar{\beta}_{i,j} + 1} \cong \hat{\beta}_{i,j}^{(r)} - \bar{\beta}_{i,j}\,; \tag{35a}$$

$$\gamma_{i}^{(r)} = \frac{\hat{\gamma}_{i}^{(r)} - \bar{\gamma}_{i}}{\bar{\gamma}_{i} + 1} \cong \hat{\gamma}_{i}^{(r)} - \bar{\gamma}_{i}\,. \tag{35b}$$

in which $\beta_{i,j}^{(r)}$ and $\gamma_{i}^{(r)}$ are the rth realisations of the elements of the random matrices $\boldsymbol{\beta}$ and $\boldsymbol{\gamma}$. These realisations can finally be used to empirically construct the marginal CDF (cumulative distribution function), which in turn can be interpolated with quantile functions described by piecewise splines or best-fitted with appropriate analytical models, e.g. Gaussian, log-normal, type-C Gram-Charlier series expansion [43], etcetera. The latter can be used to evaluate the statistics of interest, e.g. the ℓth statistical moment of the kth random variable α_k can be evaluated as:

$$\mathbb{E}\left[\alpha_k^{\ell}\right] = \int_{-\infty}^{+\infty} \alpha^{\ell}\,\mathrm{d}F_{\alpha k}(\alpha)\,, \tag{36}$$

where $F_{\alpha k}(\alpha)$ is the marginal CDF constructed for the generic random variable $\alpha_k = \beta_{i,j}$, γ_i or θ_i.

4. Perturbative methods in the modal space

4.1. Second-order perturbation

In line with the uncertainty model detailed in the previous section, a second-order perturbation approach, formulated in the reduced modal subspace, is presented herein.

Series expansion of the stochastic modal matrices about $\alpha_i = 0$, $i = 1, \ldots, \mathcal{N}$ and retaining up-to second order terms gives:

$$\begin{aligned}
\boldsymbol{\Phi}(\boldsymbol{\alpha}) &\cong \boldsymbol{\Phi}_0 + \boldsymbol{\Phi}_i\alpha_i + \boldsymbol{\Phi}_{i,j}\alpha_i\alpha_j = \bar{\boldsymbol{\Phi}} + \boldsymbol{\Phi}_i\alpha_i\,;\\
\boldsymbol{\Omega}(\boldsymbol{\alpha}) &\cong \boldsymbol{\Omega}_0 + \boldsymbol{\Omega}_i\alpha_i + \boldsymbol{\Omega}_{i,j}\alpha_i\alpha_j = \bar{\boldsymbol{\Omega}} + \boldsymbol{\Omega}_i\alpha_i\,;\\
\boldsymbol{\zeta}(\boldsymbol{\alpha}) &\cong \boldsymbol{\zeta}_0 + \boldsymbol{\zeta}_i\alpha_i + \boldsymbol{\zeta}_{i,j}\alpha_i\alpha_j = \bar{\boldsymbol{\zeta}} + \boldsymbol{\zeta}_i\alpha_i\,,
\end{aligned} \tag{37}$$

where $\boldsymbol{\Phi}_0 = \boldsymbol{\Phi}(\boldsymbol{\alpha})\,|_{\boldsymbol{\alpha}=\mathbf{0}_{\mathcal{N}}} = \bar{\boldsymbol{\Phi}}$, $\boldsymbol{\Omega}_0 = \boldsymbol{\Omega}(\boldsymbol{\alpha})\,|_{\boldsymbol{\alpha}=\mathbf{0}_{\mathcal{N}}} = \bar{\boldsymbol{\Omega}}$ and $\boldsymbol{\zeta}_0 = \boldsymbol{\zeta}(\boldsymbol{\alpha})\,|_{\boldsymbol{\alpha}=\mathbf{0}_{\mathcal{N}}} = \bar{\boldsymbol{\zeta}}$, $\mathbf{0}_{\mathcal{N}} = \mathbf{O}_{\mathcal{N}\times 1}$ being a $\mathcal{N}$-dimensional zero vector and summation is once again implied. It is noted that the terms $\boldsymbol{\Phi}_{i,j}$, $\boldsymbol{\Omega}_{i,j}$ and $\boldsymbol{\zeta}_{i,j}$ vanish, unless second-order terms are included in Eq. (27).

Substitution of Eq. (37) in Eq. (32) then gives:

$$\begin{aligned}
\mathbf{m}(\boldsymbol{\alpha}) &= \mathbf{I}_m + \boldsymbol{\Phi}_i^\top \bar{\mathbf{M}} \bar{\boldsymbol{\Phi}}\, \alpha_i + \bar{\boldsymbol{\Phi}}^\top \bar{\mathbf{M}} \boldsymbol{\Phi}_i\, \alpha_i + \bar{\boldsymbol{\Phi}}^\top \bar{\mathbf{M}} \boldsymbol{\Phi}_i \boldsymbol{\Phi}_j^\top \bar{\mathbf{M}} \bar{\boldsymbol{\Phi}}\, \alpha_i \alpha_j \,; \\
\mathbf{k}(\boldsymbol{\alpha}) &= \bar{\boldsymbol{\Omega}}^2 + \bar{\boldsymbol{\Omega}}^2 \boldsymbol{\Phi}_i^\top \bar{\mathbf{M}} \bar{\boldsymbol{\Phi}}\, \alpha_i + \bar{\boldsymbol{\Omega}} \boldsymbol{\Omega}_i\, \alpha_i + \boldsymbol{\Omega}_i \bar{\boldsymbol{\Omega}}\, \alpha_i + \bar{\boldsymbol{\Phi}}^\top \bar{\mathbf{M}} \boldsymbol{\Phi}_i \bar{\boldsymbol{\Omega}}^2\, \alpha_i + \bar{\boldsymbol{\Omega}} \boldsymbol{\Omega}_i \boldsymbol{\Phi}_j^\top \bar{\mathbf{M}} \bar{\boldsymbol{\Phi}}\, \alpha_i \alpha_j \\
&\quad + \boldsymbol{\Omega}_i \bar{\boldsymbol{\Omega}} \boldsymbol{\Phi}_j^\top \bar{\mathbf{M}} \bar{\boldsymbol{\Phi}}\, \alpha_i \alpha_j + \boldsymbol{\Omega}_i \boldsymbol{\Omega}_j\, \alpha_i \alpha_j + \bar{\boldsymbol{\Phi}}^\top \bar{\mathbf{M}} \boldsymbol{\Phi}_i \bar{\boldsymbol{\Omega}}^2 \boldsymbol{\Phi}_j^\top \bar{\mathbf{M}} \bar{\boldsymbol{\Phi}}\, \alpha_i \alpha_j + \bar{\boldsymbol{\Phi}}^\top \bar{\mathbf{M}} \boldsymbol{\Phi}_i \bar{\boldsymbol{\Omega}} \boldsymbol{\Omega}_j\, \alpha_i \alpha_j \\
&\quad + \bar{\boldsymbol{\Phi}}^\top \bar{\mathbf{M}} \boldsymbol{\Phi}_i \boldsymbol{\Omega}_j \bar{\boldsymbol{\Omega}}\, \alpha_i \alpha_j \,; \\
\mathbf{c}(\boldsymbol{\alpha}) &= \bar{\boldsymbol{\Xi}} + \bar{\boldsymbol{\Xi}} \boldsymbol{\Phi}_i^\top \bar{\mathbf{M}} \bar{\boldsymbol{\Phi}}\, \alpha_i + 2\bar{\boldsymbol{\zeta}} \boldsymbol{\Omega}_i\, \alpha_i + 2\boldsymbol{\zeta}_i \bar{\boldsymbol{\Omega}}\, \alpha_i + \bar{\boldsymbol{\Phi}}^\top \bar{\mathbf{M}} \boldsymbol{\Phi}_i \bar{\boldsymbol{\Xi}}\, \alpha_i + 2\bar{\boldsymbol{\zeta}} \boldsymbol{\Omega}_i \boldsymbol{\Phi}_j^\top \bar{\mathbf{M}} \bar{\boldsymbol{\Phi}}\, \alpha_i \alpha_j \\
&\quad + 2\boldsymbol{\zeta}_i \bar{\boldsymbol{\Omega}} \boldsymbol{\Phi}_j^\top \bar{\mathbf{M}} \bar{\boldsymbol{\Phi}}\, \alpha_i \alpha_j + 2\boldsymbol{\zeta}_i \boldsymbol{\Omega}_j\, \alpha_i \alpha_j + \bar{\boldsymbol{\Phi}}^\top \bar{\mathbf{M}} \boldsymbol{\Phi}_i \bar{\boldsymbol{\Xi}} \boldsymbol{\Phi}_j^\top \bar{\mathbf{M}} \bar{\boldsymbol{\Phi}}\, \alpha_i \alpha_j + \bar{\boldsymbol{\Phi}}^\top \bar{\mathbf{M}} \boldsymbol{\Phi}_i 2\bar{\boldsymbol{\zeta}} \boldsymbol{\Omega}_j\, \alpha_i \alpha_j \\
&\quad + \bar{\boldsymbol{\Phi}}^\top \bar{\mathbf{M}} \boldsymbol{\Phi}_i 2\boldsymbol{\zeta}_j \bar{\boldsymbol{\Omega}}\, \alpha_i \alpha_j \,;
\end{aligned} \tag{38}$$

where, in line with the conventional perturbation approach, high-order terms arising from products have been neglected.

Eq. (6), (7) and (10) still hold here. Series expansion of the dynamic matrix, and load and response vectors in Eq. (12), then gives:

$$\begin{aligned}
&\mathbf{D}_0 = \begin{bmatrix} \mathbf{O}_{m\times m} & \mathbf{I}_m \\ -\bar{\boldsymbol{\Omega}}^2 & -\bar{\boldsymbol{\Xi}} \end{bmatrix} \,; \quad \mathbf{D}_i = \begin{bmatrix} \mathbf{O}_{m\times m} & \mathbf{O}_{m\times m} \\ \mathbf{d}_i^k & \mathbf{d}_i^c \end{bmatrix} \,; \quad \mathbf{D}_{i,j} = \begin{bmatrix} \mathbf{O}_{m\times m} & \mathbf{O}_{m\times m} \\ \mathbf{d}_{i,j}^k & \mathbf{d}_{i,j}^c \end{bmatrix} \,; \\
&\mathbf{V}_0 = \begin{bmatrix} \mathbf{O}_{m\times m} \\ \mathbf{I}_m \end{bmatrix} \,; \quad \mathbf{V}_i = \begin{bmatrix} \mathbf{O}_{m\times m} \\ \boldsymbol{\mu}_i \end{bmatrix} \,; \quad \mathbf{V}_{i,j} = \begin{bmatrix} \mathbf{O}_{m\times m} \\ \boldsymbol{\mu}_{i,j} \end{bmatrix} \,.
\end{aligned} \tag{39}$$

The associated first-order terms read:

$$\begin{aligned}
\mathbf{d}_i^k &= -\bar{\boldsymbol{\Omega}}^2 \boldsymbol{\Phi}_i^\top \bar{\mathbf{M}} \bar{\boldsymbol{\Phi}} - \bar{\boldsymbol{\Omega}} \boldsymbol{\Omega}_i - \boldsymbol{\Omega}_i \bar{\boldsymbol{\Omega}} - \bar{\boldsymbol{\Phi}}^\top \bar{\mathbf{M}} \boldsymbol{\Phi}_i \bar{\boldsymbol{\Omega}}^2 - \boldsymbol{\mu}_i \bar{\boldsymbol{\Omega}}^2 \,; \\
\mathbf{d}_i^c &= -\bar{\boldsymbol{\Xi}} \boldsymbol{\Phi}_i^\top \bar{\mathbf{M}} \bar{\boldsymbol{\Phi}} - 2\bar{\boldsymbol{\zeta}} \boldsymbol{\Omega}_i - 2\boldsymbol{\zeta}_i \bar{\boldsymbol{\Omega}} - \bar{\boldsymbol{\Phi}}^\top \bar{\mathbf{M}} \boldsymbol{\Phi}_i \bar{\boldsymbol{\Xi}} - \boldsymbol{\mu}_i \bar{\boldsymbol{\Xi}} \,; \\
\boldsymbol{\mu}_i &= -\mathbf{m}_i \,;
\end{aligned} \tag{40}$$

where $\mathbf{m}_i = \boldsymbol{\Phi}_i^\top \bar{\mathbf{M}} \bar{\boldsymbol{\Phi}} + \bar{\boldsymbol{\Phi}}^\top \bar{\mathbf{M}} \boldsymbol{\Phi}_i$ represents the first-order partial derivative of the reduced mass matrix.

Second-order terms take the following form:

$$\begin{aligned}
\mathbf{d}_{i,j}^k &= -\bar{\boldsymbol{\Omega}} \boldsymbol{\Omega}_i \boldsymbol{\Phi}_j^\top \bar{\mathbf{M}} \bar{\boldsymbol{\Phi}} - \boldsymbol{\Omega}_i \bar{\boldsymbol{\Omega}} \boldsymbol{\Phi}_j^\top \bar{\mathbf{M}} \bar{\boldsymbol{\Phi}} - \boldsymbol{\Omega}_i \boldsymbol{\Omega}_j - \bar{\boldsymbol{\Phi}}^\top \bar{\mathbf{M}} \boldsymbol{\Phi}_i \bar{\boldsymbol{\Omega}}^2 \boldsymbol{\Phi}_j^\top \bar{\mathbf{M}} \bar{\boldsymbol{\Phi}} - \bar{\boldsymbol{\Phi}}^\top \bar{\mathbf{M}} \boldsymbol{\Phi}_i \bar{\boldsymbol{\Omega}} \boldsymbol{\Omega}_j - \bar{\boldsymbol{\Phi}}^\top \bar{\mathbf{M}} \boldsymbol{\Phi}_i \boldsymbol{\Omega}_j \bar{\boldsymbol{\Omega}} \\
&\quad - \boldsymbol{\mu}_i \bar{\boldsymbol{\Omega}}^2 \boldsymbol{\Phi}_j^\top \bar{\mathbf{M}} \bar{\boldsymbol{\Phi}} - \boldsymbol{\mu}_i \bar{\boldsymbol{\Omega}} \boldsymbol{\Omega}_j - \boldsymbol{\mu}_i \boldsymbol{\Omega}_j \bar{\boldsymbol{\Omega}} - \boldsymbol{\mu}_i \bar{\boldsymbol{\Phi}}^\top \bar{\mathbf{M}} \boldsymbol{\Phi}_j \bar{\boldsymbol{\Omega}}^2 - \boldsymbol{\mu}_{i,j} \bar{\boldsymbol{\Omega}}^2 \,; \\
\mathbf{d}_{i,j}^c &= -2\bar{\boldsymbol{\zeta}} \boldsymbol{\Omega}_i \boldsymbol{\Phi}_j^\top \bar{\mathbf{M}} \bar{\boldsymbol{\Phi}} - 2\boldsymbol{\zeta}_i \bar{\boldsymbol{\Omega}} \boldsymbol{\Phi}_j^\top \bar{\mathbf{M}} \bar{\boldsymbol{\Phi}} - 2\boldsymbol{\zeta}_i \boldsymbol{\Omega}_j - \bar{\boldsymbol{\Phi}}^\top \bar{\mathbf{M}} \boldsymbol{\Phi}_i \bar{\boldsymbol{\Xi}} \boldsymbol{\Phi}_j^\top \bar{\mathbf{M}} \bar{\boldsymbol{\Phi}} - 2\bar{\boldsymbol{\Phi}}^\top \bar{\mathbf{M}} \boldsymbol{\Phi}_i \bar{\boldsymbol{\zeta}} \boldsymbol{\Omega}_j - 2\bar{\boldsymbol{\Phi}}^\top \bar{\mathbf{M}} \boldsymbol{\Phi}_i \boldsymbol{\zeta}_j \bar{\boldsymbol{\Omega}} \\
&\quad - \boldsymbol{\mu}_i \bar{\boldsymbol{\Xi}} \boldsymbol{\Phi}_j^\top \bar{\mathbf{M}} \bar{\boldsymbol{\Phi}} - 2\boldsymbol{\mu}_i \bar{\boldsymbol{\zeta}} \boldsymbol{\Omega}_j - 2\boldsymbol{\mu}_i \boldsymbol{\zeta}_j \bar{\boldsymbol{\Omega}} - \boldsymbol{\mu}_i \bar{\boldsymbol{\Phi}}^\top \bar{\mathbf{M}} \boldsymbol{\Phi}_j \bar{\boldsymbol{\Xi}} - \boldsymbol{\mu}_{i,j} \bar{\boldsymbol{\Xi}} \,; \\
\boldsymbol{\mu}_{i,j} &= \frac{1}{2} \left(\mathbf{m}_i \mathbf{m}_j + \mathbf{m}_j \mathbf{m}_i - \mathbf{m}_{i,j} \right) \,,
\end{aligned} \tag{41}$$

where $\mathbf{m}_{i,j} = \bar{\boldsymbol{\Phi}}^\top \bar{\mathbf{M}} (\boldsymbol{\Phi}_i \boldsymbol{\Phi}_j^\top + \boldsymbol{\Phi}_j \boldsymbol{\Phi}_i^\top) \bar{\mathbf{M}} \bar{\boldsymbol{\Phi}}$.

A reduced system of $1 + \mathcal{N} + \mathcal{N}^2$ deterministic UP equations in state-space form is finally obtained, similarly to Eq. (13), where $\mathcal{N}$ is used in place of N, whose numerical solution with the piecewise exact method (PEM) [15, 44] can be calculated as:

$$\mathbf{z}_0(t_{k+1}) = \boldsymbol{\Theta}(\Delta t)\, \mathbf{z}_0(t_k) + \boldsymbol{\Gamma}_0(\Delta t)\, \mathbf{V}_0\, \mathbf{F}(t_k) + \boldsymbol{\Gamma}_1(\Delta t)\, \mathbf{V}_0\, \mathbf{F}(t_{k+1}) \,; \tag{42a}$$

$$\mathbf{z}_i(t_{k+1}) = \boldsymbol{\Theta}(\Delta t) \mathbf{z}_i(t_k) + \boldsymbol{\Gamma}_0(\Delta t) \left[\mathbf{D}_i\, \mathbf{z}_0(t_k) + \mathbf{V}_i\, \mathbf{F}(t_k) \right] + \boldsymbol{\Gamma}_1(\Delta t) \left[\mathbf{D}_i\, \mathbf{z}_0(t_{k+1}) + \mathbf{V}_i\, \mathbf{F}(t_{k+1}) \right] \,; \tag{42b}$$

$$\begin{aligned}
\mathbf{z}_{i,j}(t_{k+1}) &= \boldsymbol{\Theta}(\Delta t)\, \mathbf{z}_{i,j}(t_k) + \boldsymbol{\Gamma}_0(\Delta t) \left[\mathbf{D}_i\, \mathbf{z}_j(t_k) + \mathbf{D}_{i,j}\, \mathbf{z}_0(t_k) + \mathbf{V}_{i,j}\, \mathbf{F}(t_k) \right] \\
&\quad + \boldsymbol{\Gamma}_1(\Delta t) \left[\mathbf{D}_i\, \mathbf{z}_j(t_{k+1}) + \mathbf{D}_{i,j}\, \mathbf{z}_0(t_{k+1}) + \mathbf{V}_{i,j}\, \mathbf{F}(t_{k+1}) \right] \,,
\end{aligned} \tag{42c}$$

where Δt is the time step used to discretise the numerical solution, $t_k = k\,\Delta t$, with $k \geq 0$, is the kth discrete time instant, $\boldsymbol{\Theta}(\Delta t) = \exp\left[\mathbf{D}_0\,\Delta t\right]$ is the $(m \times m)$ transition matrix in the reduced modal space, $\exp[\cdot]$ denoting the matrix exponential function, and $\boldsymbol{\Gamma}_0$ and $\boldsymbol{\Gamma}_1$ are $(m \times m)$ load matrices, as defined in Appendix A.2.

Once the deterministic time histories of the state-space vectors $\mathbf{z}_0(t_k)$, $\mathbf{z}_i(t_k)$ and $\mathbf{z}_{i,j}(t_k)$ have been calculated, the statistics of the structural response can be expressed as in Eqs. (14) and (15). It is worth stressing here that Eqs. (42) are particularly appealing from a computational point of view as the numerical calculation of the $\mathcal{N}$ first-order sensitivity vectors $\mathbf{z}_i(t_k)$ and the $\mathcal{N}^2$ second-order sensitivity vectors $\mathbf{z}_{i,j}(t_k)$ can be easily parallelised.

4.2. Improved perturbation variant

In this subsection, the formulation of the improved variant for the proposed uncertainty model is detailed. Similarly to Eqs. (16) to (18) in the geometrical space, the stochastic matrices for the problem in hand can be expressed as follows:

$$\begin{aligned}
\boldsymbol{\Phi}\,(\boldsymbol{\alpha}) &\cong \boldsymbol{\Phi}_0 + \boldsymbol{\Phi}_{i,j}\,\mathbb{E}[\alpha_i\alpha_j] + \boldsymbol{\Phi}_i\alpha_i = \bar{\boldsymbol{\Phi}} + \boldsymbol{\Phi}_i\alpha_i\,;\\
\boldsymbol{\Omega}\,(\boldsymbol{\alpha}) &\cong \boldsymbol{\Omega}_0 + \boldsymbol{\Omega}_{i,j}\,\mathbb{E}[\alpha_i\alpha_j] + \boldsymbol{\Omega}_i\alpha_i = \bar{\boldsymbol{\Omega}} + \boldsymbol{\Omega}_i\alpha_i\,;\\
\boldsymbol{\zeta}\,(\boldsymbol{\alpha}) &\cong \boldsymbol{\zeta}_0 + \boldsymbol{\zeta}_{i,j}\,\mathbb{E}[\alpha_i\alpha_j] + \boldsymbol{\zeta}_i\alpha_i = \bar{\boldsymbol{\zeta}} + \boldsymbol{\zeta}_i\alpha_i\,,
\end{aligned} \tag{43}$$

where, owing to the linearity of the proposed randomisation scheme (see Eq. (27)), second-order terms vanish; therefore, the expansions of Eqs. (43) coincide with those of Eq. (37), leading to Eqs. (38).

Casting in state-space form, Eqs. (10) and (24) still hold here, with:

$$\bar{\mathbf{D}} = \begin{bmatrix} \mathbf{O}_{m\times m} & \mathbf{I}_m \\ \bar{\mathbf{d}}^k & \bar{\mathbf{d}}^c \end{bmatrix}\,;\quad \mathbf{D}_i = \begin{bmatrix} \mathbf{O}_{m\times m} & \mathbf{O}_{m\times m} \\ \hat{\mathbf{d}}_i^k & \hat{\mathbf{d}}_i^c \end{bmatrix}\,;\quad \bar{\mathbf{V}} = \begin{bmatrix} \mathbf{O}_{m\times m} \\ \bar{\boldsymbol{\mu}} \end{bmatrix}\,, \tag{44}$$

where:

$$\begin{aligned}
\bar{\mathbf{d}}^k =& -\bar{\boldsymbol{\mu}}\,\bar{\boldsymbol{\Omega}}^2 - \Big(\bar{\boldsymbol{\mu}}\,\bar{\boldsymbol{\Omega}}\boldsymbol{\Omega}_i\boldsymbol{\Phi}_j^{\top}\bar{\mathbf{M}}\bar{\boldsymbol{\Phi}} + \bar{\boldsymbol{\mu}}\,\boldsymbol{\Omega}_i\bar{\boldsymbol{\Omega}}\boldsymbol{\Phi}_j^{\top}\bar{\mathbf{M}}\bar{\boldsymbol{\Phi}} + \bar{\boldsymbol{\mu}}\,\boldsymbol{\Omega}_i\boldsymbol{\Omega}_j + \bar{\boldsymbol{\mu}}\,\bar{\boldsymbol{\Phi}}^{\top}\bar{\mathbf{M}}\boldsymbol{\Phi}_i\bar{\boldsymbol{\Omega}}^2\boldsymbol{\Phi}_j^{\top}\bar{\mathbf{M}}\bar{\boldsymbol{\Phi}} + \bar{\boldsymbol{\mu}}\,\bar{\boldsymbol{\Phi}}^{\top}\bar{\mathbf{M}}\boldsymbol{\Phi}_i\bar{\boldsymbol{\Omega}}\boldsymbol{\Omega}_j\\
&+ \bar{\boldsymbol{\mu}}\,\bar{\boldsymbol{\Phi}}^{\top}\bar{\mathbf{M}}\boldsymbol{\Phi}_i\boldsymbol{\Omega}_j\bar{\boldsymbol{\Omega}} + \boldsymbol{\mu}_i\bar{\boldsymbol{\Omega}}^2\boldsymbol{\Phi}_j^{\top}\bar{\mathbf{M}}\bar{\boldsymbol{\Phi}} + \boldsymbol{\mu}_i\bar{\boldsymbol{\Omega}}\boldsymbol{\Omega}_j + \boldsymbol{\mu}_i\boldsymbol{\Omega}_j\bar{\boldsymbol{\Omega}} + \boldsymbol{\mu}_i\bar{\boldsymbol{\Phi}}^{\top}\bar{\mathbf{M}}\boldsymbol{\Phi}_j\bar{\boldsymbol{\Omega}}^2\Big)\mathbb{E}[\alpha_i\alpha_j]\,;\\
\bar{\mathbf{d}}^c =& -\bar{\boldsymbol{\mu}}\,\bar{\boldsymbol{\Xi}} - \Big(\bar{\boldsymbol{\mu}}2\bar{\boldsymbol{\zeta}}\boldsymbol{\Omega}_i\boldsymbol{\Phi}_j^{\top}\bar{\mathbf{M}}\bar{\boldsymbol{\Phi}} + \bar{\boldsymbol{\mu}}2\boldsymbol{\zeta}_i\bar{\boldsymbol{\Omega}}\boldsymbol{\Phi}_j^{\top}\bar{\mathbf{M}}\bar{\boldsymbol{\Phi}} + \bar{\boldsymbol{\mu}}2\boldsymbol{\zeta}_i\boldsymbol{\Omega}_j + \bar{\boldsymbol{\mu}}\,\bar{\boldsymbol{\Phi}}^{\top}\bar{\mathbf{M}}\boldsymbol{\Phi}_i\bar{\boldsymbol{\Xi}}\boldsymbol{\Phi}_j^{\top}\bar{\mathbf{M}}\bar{\boldsymbol{\Phi}} + \bar{\boldsymbol{\mu}}\,\bar{\boldsymbol{\Phi}}^{\top}\bar{\mathbf{M}}\boldsymbol{\Phi}_i2\bar{\boldsymbol{\zeta}}\boldsymbol{\Omega}_j\\
&+ \bar{\boldsymbol{\mu}}\,\bar{\boldsymbol{\Phi}}^{\top}\bar{\mathbf{M}}\boldsymbol{\Phi}_i2\boldsymbol{\zeta}_j\bar{\boldsymbol{\Omega}} + \boldsymbol{\mu}_i\bar{\boldsymbol{\Xi}}\boldsymbol{\Phi}_j^{\top}\bar{\mathbf{M}}\bar{\boldsymbol{\Phi}} + \boldsymbol{\mu}_i2\bar{\boldsymbol{\zeta}}\boldsymbol{\Omega}_j + \boldsymbol{\mu}_i2\boldsymbol{\zeta}_j\bar{\boldsymbol{\Omega}} + \boldsymbol{\mu}_i\bar{\boldsymbol{\Phi}}^{\top}\bar{\mathbf{M}}\boldsymbol{\Phi}_j\bar{\boldsymbol{\Xi}}\Big)\mathbb{E}[\alpha_i\alpha_j]\,;\\
\bar{\boldsymbol{\mu}} =& \mathbf{I}_m + \boldsymbol{\mu}_{i,j}\mathbb{E}[\alpha_i\alpha_j]\,,
\end{aligned} \tag{45}$$

and

$$\begin{aligned}
\hat{\mathbf{d}}_i^k &= -\bar{\boldsymbol{\mu}}\,\bar{\boldsymbol{\Omega}}^2\boldsymbol{\Phi}_i^{\top}\bar{\mathbf{M}}\bar{\boldsymbol{\Phi}} - \bar{\boldsymbol{\mu}}\,\bar{\boldsymbol{\Omega}}\boldsymbol{\Omega}_i - \bar{\boldsymbol{\mu}}\,\boldsymbol{\Omega}_i\bar{\boldsymbol{\Omega}} - \hat{\boldsymbol{\mu}}\,\bar{\boldsymbol{\Phi}}^{\top}\bar{\mathbf{M}}\boldsymbol{\Phi}_i\bar{\boldsymbol{\Omega}}^2 - \boldsymbol{\mu}_i\bar{\boldsymbol{\Omega}}^2\,;\\
\hat{\mathbf{d}}_i^c &= -\bar{\boldsymbol{\mu}}\,\bar{\boldsymbol{\Xi}}\boldsymbol{\Phi}_i^{\top}\bar{\mathbf{M}}\bar{\boldsymbol{\Phi}} - 2\,\bar{\boldsymbol{\mu}}\,\bar{\boldsymbol{\zeta}}\boldsymbol{\Omega}_i - 2\,\bar{\boldsymbol{\mu}}\,\boldsymbol{\zeta}_i\bar{\boldsymbol{\Omega}} - \bar{\boldsymbol{\mu}}\,\bar{\boldsymbol{\Phi}}^{\top}\bar{\mathbf{M}}\boldsymbol{\Phi}_i\bar{\boldsymbol{\Xi}} - \boldsymbol{\mu}_i\bar{\boldsymbol{\Xi}}\,,
\end{aligned} \tag{46}$$

and where $\mathbf{V}_i$ satisfies Eq. (39).

Following manipulations, the resulting system of $1+\mathcal{N}$ coupled UP equations in Eq. (25) is solved with the PEM. The discretised solution then takes the form [15]:

$$\bar{\mathbf{z}}(t_{k+1}) = \bar{\boldsymbol{\Theta}}(\Delta t)\,\bar{\mathbf{z}}(t_k) + \bar{\boldsymbol{\Gamma}}_0(\Delta t)\left[\mathbb{E}[\alpha_i\alpha_j]\mathbf{D}_i\,\mathbf{z}_j(t_k) + \bar{\mathbf{V}}\,\mathbf{F}(t_k)\right] + \bar{\boldsymbol{\Gamma}}_1(\Delta t)\left[\mathbb{E}[\alpha_i\alpha_j]\mathbf{D}_i\,\mathbf{z}_j(t_{k+1}) + \bar{\mathbf{V}}\,\mathbf{F}(t_{k+1})\right]\,; \tag{47a}$$

$$\mathbf{z}_i(t_{k+1}) = \bar{\boldsymbol{\Theta}}(\Delta t)\,\mathbf{z}_i(t_k) + \bar{\boldsymbol{\Gamma}}_0(\Delta t)\left[\mathbf{D}_i\,\bar{\mathbf{z}}(t_k) + \mathbf{V}_i\,\mathbf{F}(t_k)\right] + \bar{\boldsymbol{\Gamma}}_1(\Delta t)\left[\mathbf{D}_i\,\bar{\mathbf{z}}(t_{k+1}) + \mathbf{V}_i\,\mathbf{F}(t_{k+1})\right]\,. \tag{47b}$$

Substitution of Eq. (47b) into (47a), and following manipulations, one obtains:

$$\bar{\mathbf{z}}(t_{k+1}) = \bar{\boldsymbol{\Theta}}^*(\Delta t)\,\bar{\mathbf{z}}(t_k) + \mathbf{A}_i(\Delta t)\,\mathbb{E}[\alpha_i\alpha_j]\,\mathbf{z}_j(t_k) + \bar{\boldsymbol{\Gamma}}_0^*(\Delta t)\,\mathbf{F}(t_k) + \bar{\boldsymbol{\Gamma}}_1^*(\Delta t)\,\mathbf{F}(t_{k+1})\,, \tag{48}$$

where:

$$\bar{\mathbf{\Theta}}^{*}(\Delta t) = \mathbf{G}(\Delta t)^{-1}\left[\bar{\mathbf{\Theta}}(\Delta t) + \bar{\mathbf{\Gamma}}_1(\Delta t)\,\mathbf{D}_i\,\bar{\mathbf{\Gamma}}_0(\Delta t)\,\mathbf{D}_j\,\mathbb{E}[\alpha_i\alpha_j]\right]; \tag{49a}$$

$$\mathbf{A}_i(\Delta t) = \mathbf{G}(\Delta t)^{-1}\left[\bar{\mathbf{\Gamma}}_0(\Delta t)\,\mathbf{D}_i + \bar{\mathbf{\Gamma}}_1(\Delta t)\,\mathbf{D}_i\,\bar{\mathbf{\Theta}}(\Delta t)\right]; \tag{49b}$$

$$\bar{\mathbf{\Gamma}}_0^{*}(\Delta t) = \mathbf{G}(\Delta t)^{-1}\left[\bar{\mathbf{\Gamma}}_0(\Delta t)\,\bar{\mathbf{V}} + \bar{\mathbf{\Gamma}}_1(\Delta t)\,\mathbf{D}_i\,\bar{\mathbf{\Gamma}}_0(\Delta t)\,\mathbf{V}_j\,\mathbb{E}[\alpha_i\alpha_j]\right]; \tag{49c}$$

$$\bar{\mathbf{\Gamma}}_1^{*}(\Delta t) = \mathbf{G}(\Delta t)^{-1}\,\bar{\mathbf{\Gamma}}_1(\Delta t)\left[\mathbf{D}_i\,\bar{\mathbf{\Gamma}}_1(\Delta t)\,\mathbf{V}_j\mathbb{E}[\alpha_i\alpha_j] + \bar{\mathbf{V}}\right]; \tag{49d}$$

$$\mathbf{G}(\Delta t) = \mathbf{I}_{2m} - \bar{\mathbf{\Gamma}}_1(\Delta t)\,\mathbf{D}_i\,\bar{\mathbf{\Gamma}}_1(\Delta t)\,\mathbf{D}_j\,\mathbb{E}[\alpha_i\alpha_j], \tag{49e}$$

and where $\bar{\mathbf{\Theta}}(\Delta t) = \exp\left[\bar{\mathbf{D}}\Delta t\right]$, and $\bar{\mathbf{\Gamma}}_0$ and $\bar{\mathbf{\Gamma}}_1$ are calculated from $\bar{\mathbf{\Theta}}$ and $\bar{\mathbf{D}}$ as per Appendix A.2. Eq. (47b) and (48) are numerically solved and the response statistics are finally obtained through Eqs. (26).

4.3. High-order perturbation

Aimed at enhancing the accuracy of the random vibration predictions, a high-order perturbation variant is presented in what follows through an *ad hoc* extension of the second-order perturbation method. To do this, let's consider the kth-order series expansion of the stochastic modal matrices in the proposed uncertainty model (with $k \geq 3$):

$$\begin{aligned}
\mathbf{\Phi}(\boldsymbol{\alpha}) &\cong \mathbf{\Phi}_0 + \mathbf{\Phi}_i\alpha_i + \mathbf{\Phi}_{i,j}\,\alpha_i\alpha_j + \cdots + \mathbf{\Phi}_{i,j,\ldots,q}\,\alpha_i\alpha_j\ldots\alpha_q;\\
\mathbf{\Omega}(\boldsymbol{\alpha}) &\cong \mathbf{\Omega}_0 + \mathbf{\Omega}_i\alpha_i + \mathbf{\Omega}_{i,j}\,\alpha_i\alpha_j + \cdots + \mathbf{\Omega}_{i,j,\ldots,q}\,\alpha_i\alpha_j\ldots\alpha_q;\\
\boldsymbol{\zeta}(\boldsymbol{\alpha}) &\cong \boldsymbol{\zeta}_0 + \boldsymbol{\zeta}_i\alpha_i + \boldsymbol{\zeta}_{i,j}\,\alpha_i\alpha_j + \cdots + \boldsymbol{\zeta}_{i,j,\ldots,q}\,\alpha_i\alpha_j\ldots\alpha_q,
\end{aligned} \tag{50}$$

where $\{i, j, \ldots, q\}$ denotes the set of of k indexes associated with the kth-order perturbation.

Following the procedure described in §4.1, the deviation matrices in Eq. (29), as well as the mass, spectral and damping matrices in Eq. (38), are constructed taking into account Eq. (50). Series expansion of the underlying terms in the state-space Eq. (10), then gives:

$$\begin{aligned}
\mathbf{z}(t,\boldsymbol{\alpha}) &\cong \mathbf{z}_0(t) + \mathbf{z}_i(t)\,\alpha_i + \mathbf{z}_{i,j}(t)\,\alpha_i\alpha_j + \cdots + \mathbf{z}_{i,j,\ldots,q}(t)\,\alpha_i\alpha_j\ldots\alpha_q;\\
\mathbf{D}(\boldsymbol{\alpha}) &\cong \mathbf{D}_0 + \mathbf{D}_i\alpha_i + \mathbf{D}_{i,j}\,\alpha_i\alpha_j + \cdots + \mathbf{D}_{i,j,\ldots,q}\,\alpha_i\alpha_j\ldots\alpha_q;\\
\mathbf{V}(\boldsymbol{\alpha}) &\cong \mathbf{V}_0 + \mathbf{V}_i\alpha_i + \mathbf{V}_{i,j}\,\alpha_i\alpha_j + \cdots + \mathbf{V}_{i,j,\ldots,q}\,\alpha_i\alpha_j\ldots\alpha_q,
\end{aligned} \tag{51}$$

where first- and second-order dynamic matrices and load vectors satisfy Eq. (39), while the high-order ones, whose details are lengthy, are computed by means of an algorithmic procedure.

4.3.1. *Quantification of response statistics*

Upon substitution of Eq. (51) into Eq. (10) and following manipulations, a set of $n(k) = \sum_{j=0}^{k}\mathcal{N}^{j}$ deterministic UP equations in state-space form is obtained. For instance, if $m = 5$ modes of vibration are retained in the dynamic analysis, there are up-to $\mathcal{N} = 35$ random variables (see Eq. (28)), meaning that for $k = 2$, i.e. second-order perturbation, there are up-to $n(2) = 1,261$ state-space equations; they become up-to $n(3) = 44,136$ for $k = 3$ and up-to $n(4) = 1,544,761$ for $k = 4$. It is noteworthy here that: *i*) the actual number of 'dominant' random variables can be significantly less; *ii*) parallelisation and domain decomposition methods [45, 46] can be used to simultaneously solve multiple UP equations, which in turn can drastically reduce the computational time.

For the kth order perturbation, the set of $n(k)$ UP equations can be broken down in $k+1$ subsets, of increasing number; that is, the jth subset, with $0 \leq j \leq k$, consists of $\mathcal{N}^{j}$ UP equations. The first three subsets, for $j \leq 2$, are the same as in Eqs. (13); the higher-order subsets, for $j \geq 3$ can be written in the following generalised form:

$$\underbrace{\dot{\mathbf{z}}_{i,j,\ldots,p,q}}_{j\,(\leq k)\,\text{indexes}} = \mathbf{D}_0\,\mathbf{z}_{i,j,\ldots,p,q} + \mathbf{D}_i\,\mathbf{z}_{j,\ldots,p,q} + \cdots + \mathbf{D}_{i,j,\ldots,p}\mathbf{z}_q + \mathbf{D}_{i,j,\ldots,p,q}\,\mathbf{z}_0 + \mathbf{V}_{i,j,\ldots,p,q}\,\mathbf{F}(t), \tag{52}$$

where, once again, time dependency is not explicitly shown in any of the $\mathbf{z}$ vectors and j is the number of indices $\{i, j, \ldots, p, q\}$ appearing in the subset of UP equations; it is worth stressing here that each of these indices takes combinatorially the values $1, \ldots, \mathcal{N}$ and that for the particular case $j = 3$ the expressions in Eq. (52) should be

interpreted such as $j \equiv p$.

Solution to Eq. (52) with the PEM is given as :

$$\begin{aligned}\mathbf{z}_{i,j,\ldots,p,q}(t_{k+1}) &= \boldsymbol{\Theta}(\Delta t)\,\mathbf{z}_{i,j\ldots,p,q}(t_k)\\ &+\boldsymbol{\Gamma}_0(\Delta t)\left\{\mathbf{D}_i\,\mathbf{z}_{j,\ldots,p,q}(t_k)+\cdots+\mathbf{D}_{i,j,\ldots,p}\,\mathbf{z}_q(t_k)+\mathbf{D}_{i,j,\ldots,p,q}\,\mathbf{z}_0(t_k)+\mathbf{V}_{i,j,\ldots,p,q}\,\mathbf{F}(t_k)\right\}\\ &+\boldsymbol{\Gamma}_1(\Delta t)\left\{\mathbf{D}_i\,\mathbf{z}_{j,\ldots,p,q}(t_{k+1})+\cdots+\mathbf{D}_{i,j,\ldots,p}\,\mathbf{z}_q(t_{k+1})+\mathbf{D}_{i,j,\ldots,p,q}\,\mathbf{z}_0(t_{k+1})+\mathbf{V}_{i,j,\ldots,p,q}\,\mathbf{F}(t_{k+1})\right\},\end{aligned} \tag{53}$$

which extends the PEM solutions detailed as Eqs. (42).

Response statistics are finally computed as:

$$\mathbb{E}[\mathbf{z}] = \mathbf{z}_0 + \mathbf{z}_{i,i}\,\mathbb{E}[\alpha_i^2] + \cdots + \mathbf{z}_{i,j,\ldots,q}\underbrace{\mathbb{E}\left[\alpha_i\alpha_j\ldots\alpha_q\right]}_{p\text{th-order moment}}; \tag{54a}$$

$$\begin{aligned}\mathrm{Var}[\mathbf{z}] &= \mathbb{E}[\mathbf{z}\odot\mathbf{z}] - \mathbb{E}[\mathbf{z}]\odot\mathbb{E}[\mathbf{z}]\\ &= \left\{\mathbf{z}_i\odot\mathbf{z}_i\right\}\mathbb{E}[\alpha_i^2] + \cdots + \left(\mathbf{z}_{i,j,\ldots,q}\odot\mathbf{z}_{I,J,\ldots,Q}\right)\underbrace{\mathbb{E}\left[\alpha_i\alpha_j\ldots\alpha_q\alpha_I\alpha_J\ldots\alpha_Q\right]}_{(2p)\text{th-order moment}},\end{aligned} \tag{54b}$$

where Eq. (54b) is expanded following substitution of Eq. (51) and Kronecker algebra is used; the conditions $\mathbb{E}[\alpha_i] = 0$ and $\mathbb{E}[\alpha_i\alpha_j] = 0$ for $i = j$ (zero-mean, statistically independent random variables) have also been used.

In the approach presented in this subsection, $p-2$ subsets of auxiliary deterministic differential equations, associated with high-order probabilistic information, are used to obtain an improved approximation of the dynamic response of the uncertain structure. Notably, in the special case where $p = 2$, the second-order perturbation approach in modal space, presented in Section 4.1, is recovered. An unfortunate feature of the high-order perturbation variant is the susceptibility to the curse of dimensionality, with the number of equations dramatically increasing with the underlying random variables. Nevertheless, owing to the uncertainty formulation proposed in Section 3, $\mathcal{N} \ll N$, and therefore the number of additional UP equations can be kept reasonably low. Furthermore, the model does not necessarily require a fixed value of p, as each set of auxiliary equations can be adaptively used, on-demand, on the basis of convergence criteria assessed throughout computations, to either increase the level of fidelity, or resort to a lower-order scheme, thus providing flexibility to the analyst, balancing accuracy with the additional computational effort.

4.3.2. Cumulant-neglect moment approximation

A notorious difficulty is that the proposed method requires knowledge of high-order input statistical moments, which may, in general, be unavailable. Specifically, the pth-order perturbation depends on statistical moments of up-to order $2p$. It must be further noted that the full set of $\mathcal{N}^j$ statistical moments of the jth-order can be prohibitively expensive to compute and operate with, and therefore a set of

$$\binom{\mathcal{N}+j-1}{j} = \frac{(\mathcal{N}+j-1)!}{j!\,(\mathcal{N}-1)!} \tag{55}$$

unique function evaluations can be used in practice, which are subsequently manipulated and stored, by means of a compressed format through their associated descriptor mapping. This can dramatically mitigate the computational burden of the procedure; for instance, for the case of $m = 5$ modes of vibration considered above (see Subsection 4.3.1), the number of independent UP equations that need to be solved reduces to up-to $\widetilde{n}(2) = 666$ for the second-order perturbation (i.e. 47.2% less), $\widetilde{n}(3) = 8,436$ for $p = 3$ (i.e. 80.9% less) and $\widetilde{n}(4) = 82,251$ for $p = 4$ (i.e. 94.7% less UP equations).

Rather than neglecting moments of order greater than p, as is often the case with perturbative approaches, a cumulant-neglect-based technique can be used to approximate the probability distribution of the random variables α_i. Specifically, it is possible to express the statistical moments in terms of cumulants, denoted herein with $\kappa(\cdot)$. The

following relationships are indicatively provided in compact form for up-to fourth-order [47–50]:

$$\begin{aligned}
\mathbb{E}[\alpha_i] &= \kappa(\alpha_i)\,; \\
\mathbb{E}[\alpha_i\alpha_j] &= \kappa(\alpha_i,\alpha_j) - \kappa(\alpha_i)\,\kappa(\alpha_j)\,; \\
\mathbb{E}[\alpha_i\alpha_j\alpha_p] &= \kappa(\alpha_i,\alpha_j,\alpha_p) + 3\left\{\kappa(\alpha_i)\,\kappa(\alpha_j,\alpha_p)\right\}_{\mathrm{S}} + \kappa(\alpha_i)\,\kappa(\alpha_j)\,\kappa(\alpha_p)\,; \\
\mathbb{E}[\alpha_i\alpha_j\alpha_p\alpha_q] &= \kappa(\alpha_i,\alpha_j,\alpha_p,\alpha_q) + 3\left\{\kappa(\alpha_i,\alpha_j)\,\kappa(\alpha_p,\alpha_q)\right\}_{\mathrm{S}} + 4\left\{\kappa(\alpha_i)\,\kappa(\alpha_j,\alpha_p,\alpha_q)\right\}_{\mathrm{S}} \\
&\quad + 6\left\{\kappa(\alpha_i)\,\kappa(\alpha_j)\,\kappa(\alpha_p,\alpha_q)\right\}_{\mathrm{S}} + \kappa(\alpha_i)\,\kappa(\alpha_j)\,\kappa(\alpha_p)\,\kappa(\alpha_q)\,,
\end{aligned} \tag{56}$$

where i, j, p and q are integers in the interval $[1,\mathcal{N}]$, denoting the elements of $\boldsymbol{\alpha}$, and $\{\cdot\}_{\mathrm{S}}$ indicates a symmetrising operation, that is, taking the arithmetic mean of all different permuted terms with respect to the underlying arguments.

For Gaussian random variables, cumulants of order greater than two are zero, and it thus follows that high-order moments can be approximated in terms of lower ones by neglecting cumulants above a certain order ℓ, with $2 \le \ell \le k$. The approximation is exact for Gaussian input variables and admissible to other cases, provided that the probability distribution of the input variables is not strongly non-Gaussian. In practice, results can be obtained through a second-order approximation, setting $\ell = 2$, but an improvement in accuracy can be achieved by resorting to a higher level of cumulant approximation.

4.3.3. Adaptive solution implementation procedure

To apply the high-order perturbation approach presented above, an algorithmic procedure is suggested, which can be summarised as follows:

1. DECIDE the number of modes m to be retained in the analysis, the time step Δt, the number $\mathcal{N}$ of random variables (up to $m^2+2\,m$), the number k of the perturbation order (also considering the computational resources available) and the level ℓ of cumulant-neglect closure, if required.
2. DEFINE all the matrices $\mathbf{D}$ and $\mathbf{V}$ appearing in Eqs. (13) and (52), up to the kth order.
3. CALCULATE the integration operators $\boldsymbol{\Theta}(\Delta t)$, $\boldsymbol{\Gamma}_0(\Delta t)$ and $\boldsymbol{\Gamma}_1(\Delta t)$ appearing in Eq. (53); they have to be calculated only once for all subsets of UP equations (see point 4 below).
4. For $j = 1,\dots,k$, SOLVE the jth subset of UP equations, with all the required combinations of the j indexes in Eq. (53));
5. If required, APPROXIMATE the jth statistical moment of the ith input variable, $\mathbb{E}[\alpha_i^j]$, with $j \ge \ell \ge 3$, using the cumulant-neglect closure.
6. CALCULATE the second-order response statistics via Eqs. (54).
7. REPEAT points 1 to 6 until, convergence is reached.

In practice, convergence can be measured, over the whole duration of the motion of the structure, in terms of an appropriate norm of the variance of its dynamic response.

5. Spectral quantification in the modal space with polynomial chaos expansions

The perturbative-based variants presented in the previous section are suited to the second-moment response analysis for moderate levels of uncertainty in the dynamic system. They are intrusive, requiring reformulation of the governing differential equations, and the approximation error tends to cumulate over time. To alleviate some of these drawbacks and complement our investigations, a spectral, non-intrusive approach based on the polynomial chaos (PC) expansion is next employed in combination with the modal uncertainty model presented above.

Consider the mechanical system of Section 3 characterised by the reduced random matrices in Eq. (32). Let us define an interface to the model through an $\mathcal{N}$-dimensional standard normal random input vector $\boldsymbol{u} = \left\{u_1,\dots,u_{\mathcal{N}}\right\}^{\top} \in \mathbb{R}^{\mathcal{N}}$, so obtained by means of a suitable probabilistic transformation to the random vector $\boldsymbol{\alpha}$.

The state response z_k, at the kth time instant t_k, then admits the following representation on a finite-dimensional basis by a truncated PC [23]:

$$z_k \approx \sum_{\boldsymbol{i}\in\mathcal{A}} y_{\boldsymbol{i}}\,\psi_{\boldsymbol{i}}(\boldsymbol{u})\,, \tag{57}$$

where $\psi_{\boldsymbol{i}}(\boldsymbol{u}) = \prod_{j=1}^{\mathcal{N}} P_{i_j}(u_j)$ are multivariate Hermite polynomials, orthonormal with respect to $f_{\boldsymbol{u}}$, the joint probability density function of $\boldsymbol{u}$, and P_{i_j} denotes a univariate polynomial of degree i_j; furthermore, $\boldsymbol{i} = \{i_1, \ldots, i_{\mathcal{N}}\} \in \mathcal{A}$ is a multi-index, where $|\boldsymbol{i}| = \sum_{j=1}^{\mathcal{N}} i_j$ is the degree of the polynomial $\psi_{\boldsymbol{i}}$, $\mathcal{A} \subset \mathbb{N}^{\mathcal{N}}$ being a truncated set; and $y_{\boldsymbol{i}} \in \mathbb{R}$ are coefficients to be identified.

In calculating the $(\mathcal{N}+p)!/(\mathcal{N}!p!)$ coefficients, $p = \mathscr{k} - 1$ denoting the maximal degree of the retained polynomials, projection- or regression-based methods may be employed by choosing a suitable experimental design, comprising a set of full-model evaluations, and processing the associated responses [51]. For projection-based methods, the experimental design size is determined from the quadrature scheme and p. Standard multivariate quadrature, for instance, requires a set of $(p+1)^{\mathcal{N}}$ model evaluations, while the computational cost with Smolyak's sparse quadrature scheme [52] grows polynomially with $\mathcal{N}$, which can be regarded as reasonable for medium-sized dimensional problems, but becomes intractable for large values of $\mathcal{N}$. Conversely, regression-based approaches result in a fixed experimental design size and are thus employed herein in conjunction with the proposed reduced modal subspace model for the system uncertainty.

Specifically, the highly-efficient least angle regression (LAR) algorithm [30, 53] is adopted with a finite number of n_{PC} model evaluations and with samples generated by the Latin Hypercube sampling strategy. To arrive to a predictive meta-model of the response time history, a time-dependent strategy is adopted, namely, a sparse PC is constructed at a number of discrete time instants from these n_{PC} runs, with a resolution step $\Delta t_{PC} \geqslant \Delta t$.

Owing to the ortho-normality of the polynomial basis, the first two statistical moments of the response are readily available from the expansion coefficients:

$$\begin{aligned} \mathbb{E}\left[z_k\right] &= y_{\boldsymbol{0}}\,; \\ \mathrm{Var}\left[z_k\right] &= \sum_{\substack{\boldsymbol{\alpha}\in\mathcal{A} \\ \boldsymbol{\alpha}\neq\boldsymbol{0}}} y_{\boldsymbol{\alpha}}^2\,, \end{aligned} \tag{58}$$

where $y_{\boldsymbol{0}}$ denotes the coefficient associated with the constant basis term $\psi_{\boldsymbol{0}} = 1$, and where the summation is carried out on the non-constant basis elements. Finally, to extract further information on the model response, such as the full probabilistic structure, the polynomial series expansion may be sampled using Monte Carlo simulation, at reasonable computational cost.

To this end, the resulting PC representation, facilitated by the reduced set of underlying random variables in the modal subspace, treats the computational model as "black box", with independent components at discrete time instants, preventing the accumulation of errors for relatively long integration times. Nevertheless, such representation is costly and may become increasingly difficult at late time instants due to the enhanced complexity in input-output relationships.

6. Numerical applications

The analysis of linear dynamical structures affected by uncertainties has been addressed in the preceding sections, and methods formulated in the reduced modal subspace have been presented for this purpose. In this section, for validation and comparison purposes, the proposed formulations have been numerically investigated.

6.1. Multi-storey steel frame with semi-rigid connections

In the first numerical application, the seismic response of a steel frame with uncertain flexibility in the semi-rigid beam-to-column connections has been investigated. Linear rotational springs (an acceptable approximation for the so-called damage limitation requirement) are used to model the connection stiffness at the beams' ends, as depicted in Figure 2(a), where N, Q and M denote the axial force, shear force and bending moment at the generic node, respectively, while u, w and θ are the associated displacements and rotations.

The stiffness matrix for the Euler-Bernoulli beam element with rotational springs is a function of the rotational stiffness k, defined as [54]:

$$k(v) = \frac{3EI}{l}\frac{v}{1-v}\,, \tag{59}$$

where E, I and l are the Young's modulus, moment of inertia and length of the beam, respectively, and v is the dimensionless fixity factor at the generic beam's end, within the range $[0, 1]$. The two limiting cases, i.e. $k(0) = 0$ and

Table 1
Geometrical parameters of the structural elements in the first numerical application.

	Area, A $[10^{-3}\,\mathrm{m}^2]$	Moment of inertia, I $[10^{-6}\,\mathrm{m}^4]$
Beams	306	2569
Columns	27	1710
	21.8	798.9
	14.9	251.7

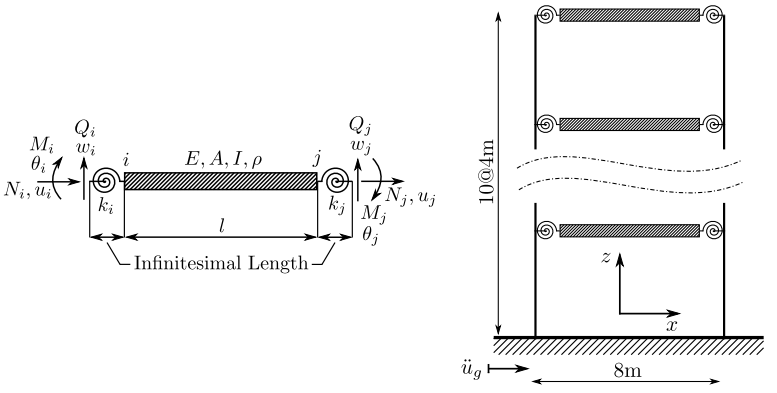

Figure 2: Beam element with rotational springs (adapted from [54]) (a) and structural frame model (b).

$\lim_{v\to 1} k(v) = +\infty$ represent a pinned connection (permitting free rotation, with no bending moment being transferred at the beam's end) or a rigid one (restraining rotation), respectively; in actual steel construction, however, the fixity factors take intermediate values, random in nature, and can significantly affect the dynamic response of semi-rigid steel frames (e.g. Refs. [55–57]).

Figure 2(b) shows the case-study model, taken from Ref. [58], consisting of a 10-storey single-bay planar frame, with uniform inter-storey heights $h = 4\,\mathrm{m}$ and bay's span $b = 8\,\mathrm{m}$. The Young's modulus is $E = 210\,\mathrm{GPa}$ and the geometrical parameters of the structural elements are reported in Table 1.

A FE model has been constructed with the commercial structural analysis software SAP2000 [59]. Having discretised each beam into two FEs of equal length $l = b/2 = 4\,\mathrm{m}$, masses $M_{\mathrm{top}} = 3\,\mathrm{Mg}$ have been lumped at the three nodes of the top storey and masses $M = 4\,\mathrm{Mg}$ at the nodes each other storey, respectively, with a frame's total mass $M_{\mathrm{tot}} = 156\,\mathrm{Mg}$. For the reference configuration with $v = 0.5$, the fundamental period of vibration is $T_1 = 1.348\,\mathrm{s}$ (76% of modal mass participation); furthermore, the total number of DoFs is $n = 90$ and $m = 5$ modes were retained in the analysis, so that 96% of the modal mass participates in the direction of interest x.

The structure is subjected to a ground acceleration $\ddot{u}_{\mathrm{g}}(t)$ consisting of an idealised, full-cycle sinusoidal pulse such that $\ddot{u}_{\mathrm{g}}(t) = A_{\mathrm{g}} \sin\left(\omega_{\mathrm{g}} t\right)$ if $0 \le t \le T_{\mathrm{g}} = 2\pi/\omega_{\mathrm{g}}$ and $\ddot{u}_{\mathrm{g}}(t) = 0$ otherwise, where A_{g} and ω_{g} are the amplitude and the frequency of the pulse, respectively. This type of excitation has been extensively considered in the literature to quantify the effects of near-fault ground motions (e.g. [44, 60, 61]).

6.1.1. Model calibration

As a first step towards the application of the proposed approach, the random matrices $\boldsymbol{\beta}$ and $\boldsymbol{\gamma}$ have been characterised by means of numerical analyses using the relationships presented in Section 3.2. Specifically, the values of the rotational stiffness at the beam-to-column connections have been modelled with a set of $N = 20$ statistically independent random variables, which represent the only source of uncertainty for this example.

Each rotational stiffness k is uniformly distributed within the interval $\left[k_{\min} = k(v_{\min}), k_{\max} = k(v_{\max})\right]$, whose extreme values correspond to $v_{\min} = 0.21$ and $v_{\max} = 0.79$, respectively; accordingly, the resulting rotational stiffness has mean value $\bar{k} = \left(k_{\min} + k_{\max}\right)/2 = k(v_0)$, with $v_0 = 0.67$, and coefficient of variation $\mathrm{CoV}[k] = 0.50$.

Following the procedure detailed in Section 3.3, a MCS has been carried out with 50,000 realisations to construct

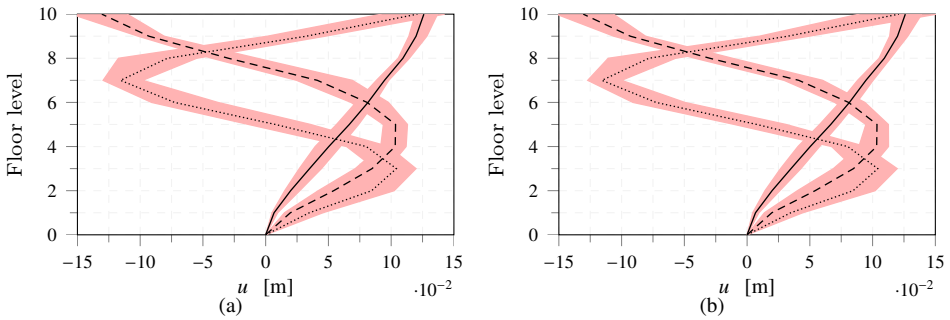

Figure 3: Randomised first three modal shapes due to uncertainty characterised in the full geometric space (a); and due to the proposed uncertainty model in the reduced modal subspace by means of 25 calibrated uncorrelated random variables simulated from empirical distributions (b).

the randomised mass and stiffness matrices of the semi-rigid frame in the geometrical space. The associated eigenvalue problem has been solved for each case, so obtaining randomised modal shapes and modal frequencies. This has been efficiently done by exploiting the open application programming interface (OAPI) of SAP2000 in conjunction with MATLAB [62], following the procedure delineated in Ref. [63], which automates the construction and analysis of the structural model as well as the customised retrieval of the required results.

In a subsequent stage, Eqs. (33) to (35) have been used to empirically construct the marginal CDFs and correlation matrix for the random variables in $\boldsymbol{\beta}$ and $\boldsymbol{\gamma}$, associated with the modal shapes and modal circular frequencies, while uniformly distributed random variables were used for the elements of the random vector $\boldsymbol{\theta}$, based on mean value $\bar{\zeta} = 0.05$, for all modes, and $\mathrm{CoV}[\zeta] = 0.2$.

It is worth noting here that the total number of random variables in the reduced modal space is $\mathcal{N} = 5^2 + 2\times 5 = 35$, meaning that $\mathcal{N} > N$ for this first numerical example; indeed, for simplicity's sake, other sources of uncertainty have been neglected in this application, e.g. the magnitude of the masses at each storey. A case where $N \gg \mathcal{N}$, as expected in real-life applications, is covered in the second numerical example.

Next, a suite of 100,000 realisations of $\mathcal{N}$ uncorrelated standard normal random variables were simulated and used to generate realisations of the dimensionless random variables in $\boldsymbol{\alpha}^{\mathsf{T}} = \left\{\boldsymbol{\beta}^{\mathsf{T}}, \boldsymbol{\gamma}^{\mathsf{T}}, \boldsymbol{\theta}^{\mathsf{T}}\right\}$, through the probabilistic transformation $\alpha_i^{(r)} = F_i^{-1}\left(\varkappa_i^{(r)}\right)$, where $F_i\left(\alpha_i\right)$ is the identified CDF of the ith random variable in the reduced modal space and the superscripted (r) denotes its rth realisation. For each case, the randomised modal matrix, spectral matrix, and matrix of modal damping ratios were constructed on the basis of Eqs. (27).

Figure 3 compares the randomised modal shapes due to uncertainties in the geometrical space (Figure 3(a)) with the ones from the calibrated proposed uncertainty model (Figure 3(b)). The black lines represent mean modal shapes, which coincide with the deterministic ones for the reference configuration, i.e. with all fixity factors assumed to be $\nu = 0.5$, and the light red ones refer to the envelope of realisations. The results visually confirm that both the proposed randomisation scheme (i.e. Eqs. (27)) and the identification procedure employed for the random variables α_i are satisfactory. It is further noted that the mean and standard deviation values of the simulated circular frequencies show percentage differences that fall within 0.05% and 1% of the target ones, respectively.

6.1.2. Analysis

The identified model parameters have been used to numerically investigate the performance of the proposed second-order, improved, and high-order perturbation variants as well as the PC approach, the latter carried out with $n_{\mathrm{PC}} = 500$ model evaluations, on the evolutionary displacement response at roof level. In this numerical application, only the case of $\mathscr{k} = 3$ has been considered for the high-order perturbation and PC solution, corresponding to a third-order truncation, as higher orders were found to result in only marginal improvements in the response statistics.

Figures 4(a)-4(c) show the time varying mean of the response for three different values of the normalised frequency parameter $\beta = \omega_{\mathrm{g}}/\omega_1$, namely 0.5, 1 and 1.5, respectively, while the amplitude of the ground acceleration, $A_{\mathrm{g}} = 1.0\,\mathrm{m/s^2}$, is the same in the three cases. The variants are compared against pertinent MCS, where the light red colour represents the envelope of 100,000 realisations. The results show distinct behaviour in the response; as expected, an increase in the amplitude of oscillations is exhibited for the tuned system with $\beta = 1$, leading to an increase in

the uncertainty propagated in the time history of the response. Overall, the mean dynamic response is satisfactorily predicted by all the four variants.

By contrast, the numerical analyses reveal different levels of accuracy in the prediction of the evolutionary variance of the dynamic response, plotted in Figures 4(d)-4(f); the associated time-varying percentage errors, quantified with respect to the MCS, are shown in Figures 4(g)-4(i), in which:

$$\varepsilon(t)\,[\%] = 100 \times \frac{\left|\mathrm{Var}\,[x(t)] - \mathrm{Var}\,[x(t)]_{\mathrm{MCS}}\right|}{\left|\mathrm{Var}\,[x(t)]_{\mathrm{MCS}}\right|}\,, \tag{60}$$

where $x(t)$ denotes the response quantity of interest (i.e. the displacement at roof level in this case), the subscript MCS marks the reference value of the variance calculated through Monte Carlo simulation, and the symbol $|\cdot|$ denotes the peak absolute value of the quantity within the vertical lines.

A cumulant-neglect second-order ($\ell = 2$) closure has been used to approximate moments of up-to sixth order arising in the third-order ($k = 3$) perturbation variant. To assess the effectiveness of this approximation, the third-order perturbation response with truncated high-order moments has been superimposed in Figures 4(g)-4(i) (depicted with dotted lines).

The results show relatively large discrepancies for the conventional and improved perturbation approaches, particularly for $t > 2.5$ s, for Figures 4(d)-4(f). The proposed high-order perturbation variant and PC solution exhibit better performance, closely resembling the MCS solution. Specifically, they appear to satisfactorily predict the second-order response statistics in all the considered cases. This observation is further supported in Figures 4(g)-4(i) with the cumulative errors consistently being kept below 10%. Notably, while the performance of the perturbative methods tends to deteriorate as time increases, this is not the case for the PC variant, which consistently shows good performance. This is due to the non-intrusive nature of the adopted PC, which prevents the cumulation of the error [31].

6.2. Simply supported bridge subjected to a moving load

The second numerical application considers the transient vibration of a simply supported beam of length L, subjected to a moving load. The problem is ruled by the following second-order partial differential equation [64]:

$$\rho A\,\ddot{u}(x,t) + D(x,t) + EI\,u''''(x,t) = P\,\delta(x - V\,t)\,, \tag{61}$$

where $u(x,t)$ is the transverse displacement at point x and time t and the superscripted prime denotes spatial derivative with respect to the abscissa x; ρA is the mass density per unit length of the beam and EI is its flexural stiffness; $D(x,t)$ is the function representing the damping force in the geometrical space; P is the intensity of the moving load, arriving at time $t = 0$, and travelling at a constant velocity V; and $\delta(\cdot)$ is the Dirac's delta function. The moving load is thus acting on the beam during the time interval $[0, t_L]$, $t_L = L/v$ being the loading time.

The modal shapes and modal frequencies are given in closed form by:

$$\varphi_i(x) = \sqrt{\frac{2}{\rho A L}}\,\sin\left(\frac{i\,\pi\,x}{L}\right)\,;\quad \omega_i = \left(\frac{i\,\pi}{L}\right)^2\sqrt{\frac{EI}{\rho A}}\,, \tag{62}$$

where φ is normalised with respect to ρA.

The modal equations of motion can be obtained by adopting the following transformation of coordinates (similar to Eq.(5)):

$$u(x,t) = \boldsymbol{\varphi}_0^{\mathsf{T}}(x)\,\mathbf{q}(t)\,, \tag{63}$$

where $\boldsymbol{\varphi}_0(x) = \left\{\varphi_1(x),\, \varphi_2(x)\,\ldots\,\varphi_m(x)\right\}^{\mathsf{T}}$ is the $(m \times 1)$ modal vector, collecting the first m modal shapes of the homogeneous beam, and $\mathbf{q}(t) = \left\{q_1(t),\, q_2(t)\,\ldots\,q_m(t)\right\}^{\mathsf{T}}$ is the $(m \times 1)$ vector of the associated modal coordinates.

Upon substitution of Eq. (63) in Eq. (61), and following manipulations, one obtains (equivalent to the deterministic version of Eq. (6), in which the presence of the random variables α_i is neglected in Eqs. (8)):

$$\mathbf{I}_m\,\ddot{\mathbf{q}}(t) + \boldsymbol{\Xi}_0\,\dot{\mathbf{q}}(t) + \boldsymbol{\Omega}_0^2\,\mathbf{q}(t) = \mathbf{F}(t)\,, \tag{64}$$

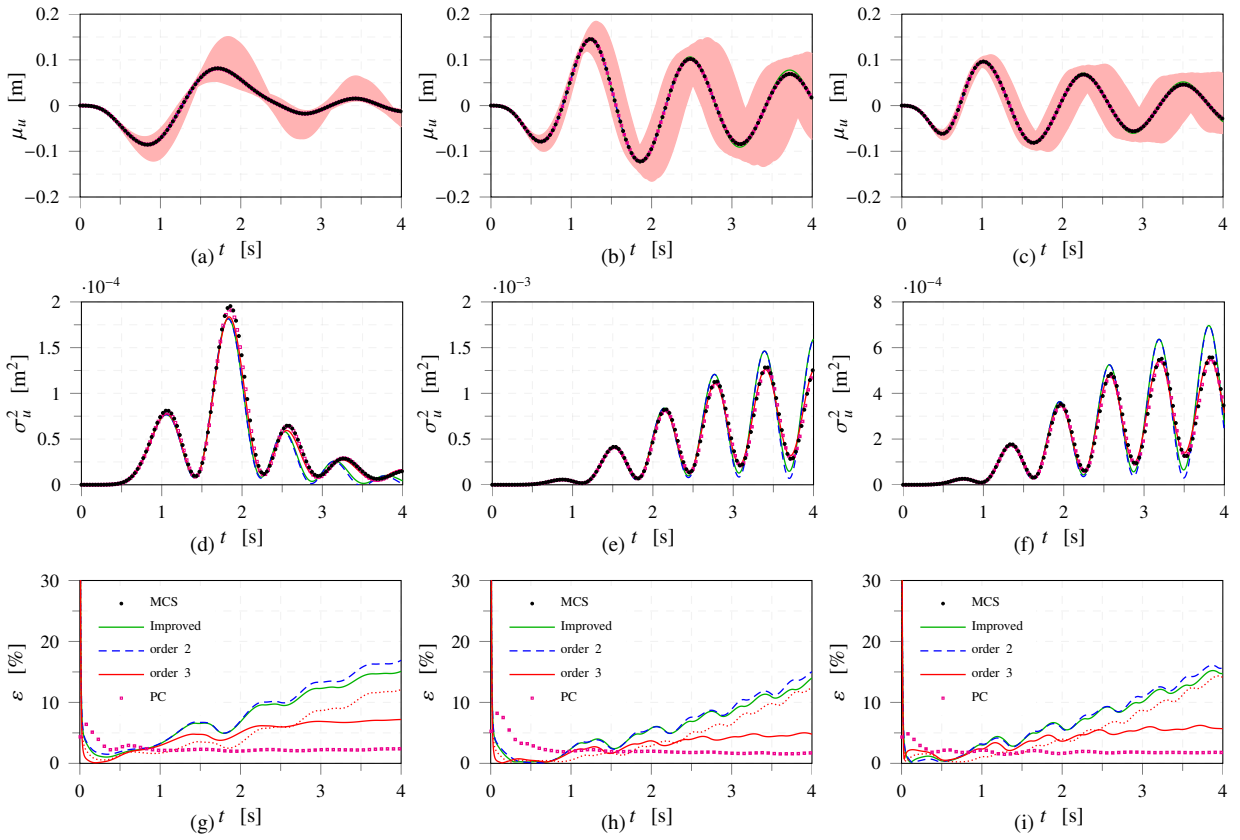

Figure 4: Displacement at roof level due to uncertainty in the reduced modal subspace for a pulse-type ground excitation of $\beta = 0.5$ (left column); $\beta = 1$ (central column); and $\beta = 1.5$ (right column): evolutionary mean (top row: a, b, c); evolutionary variance (middle row: d, e, f); and cumulative errors in the response variance (bottom row: g, h, i).

where the loading vector in the reduced modal space is given by $\mathbf{F}(t) = P\,\mathbf{G}(t)$, being:

$$\mathbf{G}(t) = \boldsymbol{\varphi}_0^{\top}(V\,t) = \sqrt{\frac{2}{\rho A\,L}} \begin{Bmatrix} \sin(\pi\,V\,t/L) \\ \sin(2\,\pi\,V\,t/L) \\ \vdots \\ \sin(m\,\pi\,V\,t/L) \end{Bmatrix}. \tag{65}$$

In line with the numerical example reported in Ref.[65], the following mechanical parameters have been selected for the beam: $L = 27.5\,\mathrm{m}$, $\rho A = 2.385\,\mathrm{Mg/m}$, and $EI = 12.425 \times 10^6\,\mathrm{kN\,m^2}$; $P = 96.53\,\mathrm{kN}$ is the magnitude of the moving load. Furthermore, $m = 3$ modes of vibration have been retained in analysis; under the reference configuration, when no random fluctuations are present, the modal circular frequencies are $\omega_1 = 29.8$, $\omega_2 = 119.2$ and $\omega_3 = 268.1\,\mathrm{rad/s}$.

6.2.1. Model calibration

To calibrate the probabilistic definition of the random variables in the reduced modal space, an auxiliary FE model was constructed, comprising of a total of 200 Euler-Bernoulli beam elements and a total of $N = 400$, independent, uniformly distributed random variables, representing uncertainty in the geometrical space, namely, in the mass density and bending stiffness of each FE, based on a coefficient of variation of 0.14 and 0.3, respectively.

A MCS was carried out with 50,000 realisations, and randomised modal shapes and spectral matrices were obtained. The marginal CDFs of the random variables in $\boldsymbol{\beta}$ and $\boldsymbol{\gamma}$ were constructed through the use of Eqs. (33) to (35). Furthermore, uniformly distributed random variables were assumed for the marginal CDFs of the random variables in

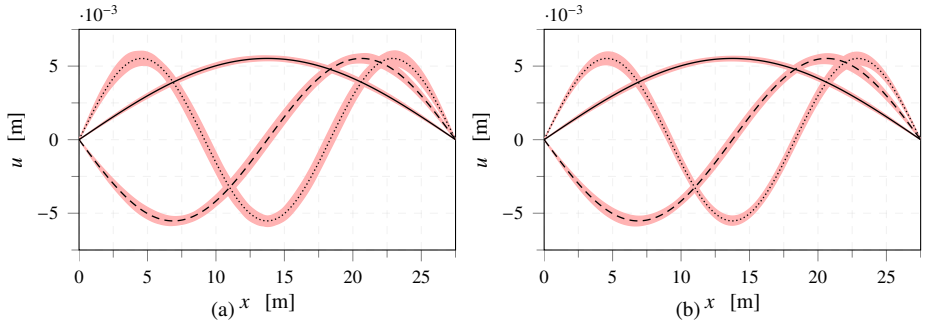

Figure 5: Randomised first three modal shapes due to uncertainty characterised in the full geometric space with $N = 400$ random variables (a); and due to the proposed uncertainty model in the reduced modal subspace by means of 9 calibrated uncorrelated random variables simulated from empirical distributions (b).

$\boldsymbol{\theta}$, based on a mean value of $\bar{\zeta} = 0.02$, for all modes, and CoV $= 0.4$, giving rise to a total of $\mathcal{N} = m^2 + 2\,m = 15$ random variables, fully characterising the uncertainty model in the reduced modal space.

A suite of 100,000 realisations of $\boldsymbol{\beta}$, $\boldsymbol{\gamma}$ and $\boldsymbol{\theta}$ were next simulated, and randomised modal matrices, spectral matrices and modal matrices of damping ratios were constructed using Eqs. (27).

The randomised modal shapes due to uncertainties in the geometrical space are shown in Figure 5(a), and are compared with the ones from the proposed model in Figure 5(b). The comparison is satisfactory, as the corresponding envelopes of realisations (light red lines) around the mean modal shapes (black lines) closely matching each other; uncertainty only appears to be slightly underestimated in the third modal shape, in the range $L/4 < x < 3\,L/4$. This is due to the fact that the proposed uncertainty model expresses spatial fluctuations in the modal shapes as linear combinations of the first m modes of vibration of the deterministic structure (see the first of Eqs.(27)), meaning that spatial patterns requiring wavelengths shorter than $\lambda_m = 2\,L/m$ are filtered out.

It is also noted that the mean and standard deviation values of the first three modal circular frequencies show percentage differences that fall within 0.01% and 0.3% of the target ones, respectively.

6.2.2. Analysis

The performance of the second-order, improved, third- ($\mathscr{k} = 3$) and fourth-order ($\mathscr{k} = 4$) perturbation, as well as the PC ($\mathscr{k} = 3$, $n_{\text{PC}} = 500$) variant, have been numerically investigated with reference to the random process $u(L/2, t)$, representing the evolutionary displacement response of the simply supported beam at midpsan.

The time varying mean of the response is shown in Figures 6(a)-6(c), when a moving load travelling at constant velocities of $V = 25$, 80 and 135 m/s is respectively considered, compared against pertinent MCS with 100,000 realisations (light red colour); the corresponding loading times are $t_L = 1.100$, 0.344 and 0.204 s. The results show an increase in the amplitude of oscillations exhibited at higher moving load velocities; the uncertainty propagated in the time history of the response also increases. All the variants accurately predict the mean response, with the exception of the improved perturbation, whose performance deteriorates after 5 cycles (i.e. $t > 1$ s) for the case of $V = 135$ m/s (Figure 6(c)).

The evolutionary variance of the response is plotted in Figures 6(d)-6(f) and cumulative percentage errors, with respect to the MCS, are presented in Figures 6(g)-6(i). Moments of up-to sixth and eighth order arising in the third and fourth order perturbation variants have been approximated by a cumulant-neglect second-order ($\varkappa = 2$) approximation. To assess the effectiveness of the approximation, the third and fourth order perturbation responses with truncated high-order moments arising are shown with dotted lines.

Large discrepancies are shown for the conventional and improved perturbations, propagating in the time histories of the response, most evident at $t > 1$ s, for Figures 6(d) and 6(f), with the proposed high-order perturbation and PC variants exhibiting improved performance, closely resembling the reference MCS. More specifically, the fourth-order perturbation and the PC solution are shown to accurately predict second-order response statistics for all cases considered. Indeed, this observation is also supported in Figures 6(g)-6(i) with the respective cumulative errors being kept below 5%. Moreover, the validity of the high-order statistical moment approximation is confirmed with the solid and dotted lines closely resembling each other early in the time history of the response.

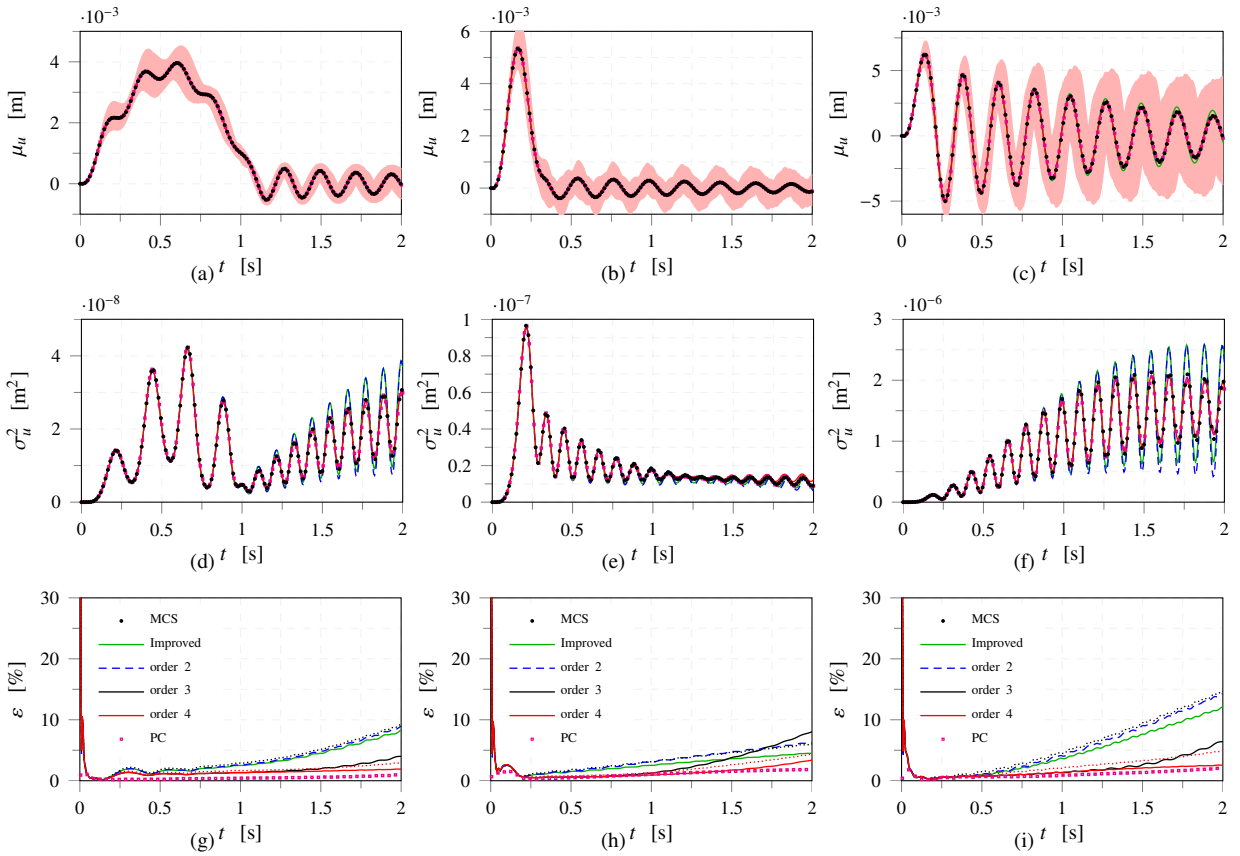

Figure 6: Midspan deflection due to uncertainty in the reduced modal subspace for a moving load travelling at a constant speed of $v = 25\,\mathrm{m/s}$ (left column); $v = 80\,\mathrm{m/s}$ (central column); and $v = 135\,\mathrm{m/s}$ (right column): evolutionary mean (top row: a, b, c); evolutionary variance (middle row: d, e, f); and cumulative errors in the response variance (bottom row: g, h, i).

Overall, the results indicate that, compared to low-order classical perturbation variants, the proposed high-order perturbation can provide a viable alternative for the second-moment response analysis of dynamical structures, with significant improvements at moderate to high levels of system uncertainty. The increase in computational effort, in practice, may be justified by means of a priori assessment of the expected gains in terms of accuracy. Sparse regression-based PC, facilitated by the modal subspace reduction, are well-suited for the spectral response quantification. Even though such representation is costly, its non-intrusive nature enables high-fidelity asynchronous examination of distinct regions in the response. Although quantification of the full probabilistic structure of the response falls beyond the scope of this work, it is noted that the numerical investigations presented exhibit non-Gaussian responses. It is finally noted that further investigations on a range of configurations, including other moving load velocities, levels of uncertainty, and input marginal distributions, have revealed that the proposed variants consistently maintain good performance.

7. Summary and conclusions

The linear dynamic analysis of structures with uncertain mechanical parameters subjected to deterministic excitation, has been addressed. In this study:

1. A model has been presented whereby system uncertainty is conveniently characterised in the reduced modal subspace rather than in the full geometrical space, with modal shapes, frequencies and damping ratios constituting the random quantities, dramatically reducing the number of underlying random variables and the size of the dynamic problem.

2. A numerical procedure has been suggested for calibrating a set of uncorrelated random variables, fully defining the proposed uncertainty model, by means of marginal distributions identified through analysis in the geometrical space and suitable probabilistic transformations; as an alternative, the random variables in the reduced modal space can be directly assumed based on the outcomes of experimental campaigns on existing structures.
3. Formulated in the reduced modal subspace, conventional second-order as well as improved perturbation variants have been presented.
4. A high-order perturbation variant has also been proposed, in-line with modern computing paradigms for on-demand computations. Based on an *ad hoc* extension of the second-order perturbation approach, the proposed method involves a set of auxiliary differential equations to be solved with the piecewise exact method (PEM). It further uses moment-cumulant relationships to approximate the high-order statistical moments of the input variable, that often might be unavailable.
5. A regression-based, non-intrusive, polynomial chaos (PC) expansion approach has been employed to complement the second-moment analysis for spectral quantification in line with the proposed modal subspace reduction.
6. Numerical investigations on a multi-storey steel frame with semi-rigid connections and a simply supported beam subjected to a moving load have confirmed the validity of the second-order, improved, high-order perturbation variants as well as the spectral approach.
    - The high-order perturbation variant has been found to outperform the conventional and improved variants in terms of accuracy, providing increased flexibility, enabling the analyst to adaptively decide the level of fidelity, thus balancing accuracy and computational cost.
    - The spectral approach has been proven effective in terms of accuracy and computational cost, allowing high-fidelity asynchronous examination of distinct regions in the response, preventing the cumulation of errors at late time instants.

Future works will consider joint eigenvalue and eigenvector statistics, i.e. accounting for the effects of cross-correlations between the random variables in the reduced modal space, as well as reliability analyses associated with extreme responses and damage cumulation.

Acknowledgement

The authors are grateful for the financial support provided by the School of Architecture, Building and Civil Engineering at Loughborough University, which has funded SK's PhD project. The authors also thank the anonymous reviewers for their constructive comments, which have contributed to strengthen the paper.

A. Appendix

A.1. Inverse matrix differentiation

Let matrix $\mathbf{G}$ be a function of α_i and α_j. Expressing $\mathbf{G}\,\mathbf{G}^{-1} = \mathbf{I}$ and making use of product rule, the first and second partial derivatives of its inverse can be expressed as follows:

$$\begin{aligned}\frac{\partial \mathbf{G}^{-1}}{\partial \alpha_i} &= -\mathbf{G}^{-1}\frac{\partial \mathbf{G}}{\partial \alpha_i}\mathbf{G}^{-1}\,;\\ \frac{\partial^2 \mathbf{G}^{-1}}{\partial \alpha_i \partial \alpha_j} &= \mathbf{G}^{-1}\frac{\partial \mathbf{G}}{\partial \alpha_i}\mathbf{G}^{-1}\frac{\partial \mathbf{G}}{\partial \alpha_j}\mathbf{G}^{-1} - \mathbf{G}^{-1}\frac{\partial^2 \mathbf{G}}{\partial \alpha_i \partial \alpha_j}\mathbf{G}^{-1} + \mathbf{G}^{-1}\frac{\partial \mathbf{G}}{\partial \alpha_j}\mathbf{G}^{-1}\frac{\partial \mathbf{G}}{\partial \alpha_i}\mathbf{G}^{-1}\,.\end{aligned} \tag{66}$$

Notably, expressions for higher derivatives can be readily obtained by means of the same process.

A.2. Piecewise Exact Method

Consider a linear second-order differential equation of the form of Eq. (6), when no fluctuations are present i.e. $\alpha_i = 0$. The state-space form is given by Eq. (13a) and the associated integral form reads [34]:

$$\mathbf{z}_0 = \boldsymbol{\Theta}(t - t_0)\,\mathbf{z}_0(t_0) + \int_{t0}^{t} \boldsymbol{\Theta}(t - \tau)\,\mathbf{V}_0\,\mathbf{F}(\tau)\,\mathrm{d}\tau\,. \tag{67}$$

The discretised solution is given by Eq. (42a), where the transition matrix $\boldsymbol{\Theta}(\Delta t) = \exp\left[\mathbf{D}_0 \Delta t\right]$, only depends on Δt, tacitly assumed sufficiently small, so that the interpolation of the forcing is satisfactory.

Furthermore the load operators $\boldsymbol{\Gamma}_0$ and $\boldsymbol{\Gamma}_1$ are given by:

$$\begin{aligned} \boldsymbol{\Gamma}_0(\Delta t) &= \left[\boldsymbol{\Theta}(\Delta t) - \mathbf{L}(\Delta t)\right] \mathbf{D}_0^{-1} ; \\ \boldsymbol{\Gamma}_1(\Delta t) &= \left[\mathbf{L}(\Delta t) - \mathbf{I}_{2m}\right] \mathbf{D}_0^{-1} , \end{aligned} \tag{68}$$

in which

$$\mathbf{L}(\Delta t) = \frac{1}{\Delta t} \left[\boldsymbol{\Theta}(\Delta t) - \mathbf{I}_{2m}\right] \mathbf{D}_0^{-1} . \tag{69}$$

It is noted that the systems in Eq. (13b) and Eq. (13c) can be solved in a similar manner.

References

[1] Shinozuka, M., 1987. Structural response variability. Journal of Engineering Mechanics 113, 825–842. doi:10.1061/(ASCE)0733-9399(1987)113:6(825).

[2] Bucher, C., Shinozuka, M., 1988. Structural response variability II. Journal of Engineering Mechanics 114, 2035–2054. doi:10.1061/(ASCE)0733-9399(1988)114:12(2035).

[3] Kardara, A., Bucher, C., Shinozuka, M., 1989. Structural response variability III. Journal of Engineering Mechanics 115, 1726–1747. doi:10.1061/(ASCE)0733-9399(1989)115:8(1726).

[4] Sofi, A., Romeo, E., Barrera, O., Cocks, A., 2019. An interval finite element method for the analysis of structures with spatially varying uncertainties. Advances in Engineering Software 128, 1–19. doi:https://doi.org/10.1016/j.advengsoft.2018.11.001.

[5] Stefanou, G., 2009. The stochastic finite element method: Past, present and future. Computer Methods in Applied Mechanics and Engineering 198, 1031–1051. doi:10.1016/j.cma.2008.11.007.

[6] Pryse, S., Kundu, A., Adhikari, S., 2018. Projection methods for stochastic dynamic systems: a frequency domain approach. Computer Methods in Applied Mechanics and Engineering 338, 412–439. doi:https://doi.org/10.1016/j.cma.2018.04.025.

[7] Feng, N., Zhang, G., Khandelwal, K., 2021. On the performance evaluation of stochastic finite elements in linear and nonlinear problems. Computers & Structures 243, 106408. doi:https://doi.org/10.1016/j.compstruc.2020.106408.

[8] Kleiber, M., Hien, T., 1992. The stochastic finite element method. John Wiley & Sons, New York.

[9] Liu, X., Zhao, X., Adhikari, S., Liu, X., 2021. Stochastic dynamic stiffness for damped taut membranes. Computers & Structures 248, 106483. doi:10.1016/j.compstruc.2021.106483.

[10] Schneider, F., Papaioannou, I., Ehre, M., Straub, D., 2020. Polynomial chaos based rational approximation in linear structural dynamics with parameter uncertainties. Computers & Structures 233, 106223. doi:doi.org/10.1016/j.compstruc.2020.106223.

[11] Katafygiotis, L., Papadimitriou, C., 1996. Dynamic response variability of structures with uncertain properties. Earthquake Engineering & Structural Dynamics 25, 775–793. doi:10.1002/(SICI)1096-9845(199608)25:8<775::AID-EQE581>3.0.CO;2-1.

[12] Kaminski, M., 2007. Generalized perturbation-based stochastic finite element method in elastostatics. Computers & Structures 85, 586–594. doi:10.1016/j.compstruc.2006.08.077.

[13] Liu, W., Belytschko, T., Mani, A., 1986. Probabilistic finite elements for nonlinear structural dynamics. Computer Methods in Applied Mechanics and Engineering 56, 61–81. doi:10.1016/0045-7825(86)90136-2.

[14] Elishakoff, I., Ren, Y., Shinozuka, M., 1995. Improved finite element method for stochastic problems. Chaos, Solitons and Fractals 5, 846–83. doi:10.1016/0960-0779(94)00157-L.

[15] Muscolino, G., Ricciardi, G., Impollonia, N., 2000. Improved dynamic analysis of structures with mechanical uncertainties under deterministic input. Probabilistic Engineering Mechanics 15, 199–212. doi:10.1016/S0266-8920(99)00021-1.

[16] Falsone, G., Impollonia, N., 2002. A new approach for the stochastic analysis of finite element modelled structures with uncertain parameters. Computer Methods in Applied Mechanics and Engineering 191, 5067–5085. doi:10.1016/S0045-7825(02)00437-1.

[17] Impollonia, N., Sofi, A., 2003. A response surface approach for the static analysis of stochastic structures with geometrical nonlinearities. Computer Methods in Applied Mechanics and Engineering 192, 4109–4129. doi:10.1016/S0045-7825(03)00379-7.

[18] Falsone, G., Ferro, G., 2007. An exact solution for the static and dynamic analysis of fe discretized uncertain structures. Computer Methods in Applied Mechanics and Engineering 196, 2390–2400. doi:10.1016/j.cma.2006.12.003.

[19] Kundu, A., Adhikari, S., 2015. Dynamic analysis of stochastic structural systems using frequency adaptive spectral functions. Probabilistic Engineering Mechanics 39, 23–38. doi:10.1016/j.probengmech.2014.11.003.

[20] Kundu, A., Adhikari, S., 2014. Transient response of structural dynamic systems with parametric uncertainty. Journal of Engineering Mechanics 140, 315–331. doi:10.1061/(ASCE)EM.1943-7889.0000643.

[21] Hua, X., Ni, Y., Chen, Z., Ko, J., 2008. An improved perturbation method for stochastic finite element model updating. International Journal for Numerical Methods in Engineering 73, 1845–1864. doi:10.1002/nme.2151.

[22] Ding, C., Tamma, K., Cui, X., Ding, Y., Li, G., Bordas, S., 2020. An nth high order perturbation-based stochastic isogeometric method and implementation for quantifying geometric uncertainty in shell structures. Advances in Engineering Software 148, 102866. doi:https://doi.org/10.1016/j.advengsoft.2020.102866.

[23] Ghanem, R., Spanos, P., 2003. Stochastic finite elements: A spectral approach. Springer, Berlin.

[24] Jacquelin, E., Adhikari, S., Sinou, J., Friswell, M., 2015. Polynomial chaos expansion and steady-state response of a class of random dynamical systems. Journal of Engineering Mechanics 141, 04014145. doi:10.1061/(ASCE)EM.1943-7889.0000856.

[25] Jacquelin, E., Dessombz, O., Sinou, J., Adhikari, S., Friswell, M., 2017. Polynomial chaos-based extended Padé expansion in structural dynamics. International Journal for Numerical Methods in Engineering 111, 1170–1191. doi:10.1002/nme.5497.

[26] Jacquelin, E., Brizard, D., Adhikari, S., Friswell, M., 2020. Time-domain response of damped stochastic multiple-degree-of-freedom systems. Journal of Engineering Mechanics 146, 06019005. doi:10.1061/(ASCE)EM.1943-7889.0001705.

[27] Babuška, I., Nobile, F., Tempone, R., 2007. A stochastic collocation method for elliptic partial differential equations with random input data. SIAM Journal on Numerical Analysis 45, 1005–34. doi:10.1137/050645142.

[28] Le Maître, O., Reagan, M., Najm, H., Ghanem, R., Knio, O., 2002. A stochastic projection method for fluid flow - II. random process. Journal of Computational Physics 181, 9–44. doi:10.1006/jcph.2002.7104.

[29] Berveiller, M., Sudret, B., Lemaire, M., 2006. Stochastic finite element: a non intrusive approach by regression. European Journal of Computational Mechanics 15, 81–92. doi:doi:10.3166/remn.15.81-92.

[30] Blatman, G., Sudret, B., 2011. Adaptive sparse polynomial chaos expansion based on least angle regression. Journal of Computational Physics 230, 2345–2367.

[31] Mai, C., Sudret, B., 2017. Surrogate models for oscillatory systems using sparse polynomial chaos expansions and stochastic time warping. SIAM/ASA Journal on Uncertainty Quantification 5, 540–571. doi:10.1137/16M1083621.

[32] Kasinos, S., Palmeri, A., Lombardo, M., 2015. Performance-based seismic analysis of light SDoF secondary substructures, in: 12th International Conference on Applications of Statistics and Probability in Civil Engineering. doi:10.14288/1.0076300.

[33] Kasinos, S., Palmeri, A., Maheshwari, S., Lombardo, M., 2017. Dynamic analysis of steel frames with uncertain semi-rigid connections, in: 12th International Conference on Structural Safety and Reliability.

[34] Kasinos, S., 2018. Seismic response analysis of linear and nonlinear secondary structures. PhD thesis, Loughborough University.

[35] Sudret, B., Der Kiureghian, A., 2000. Stochastic finite element methods and reliability. A state-of-the-art report. Technical Report UCB/SEMM-2000/08, University of California, Berkeley.

[36] Nalecz, A., Wicher, J., 1988. Design sensitivity analysis of mechanical systems in frequency domain. Journal of Sound and Vibration 120, 517–526. doi:10.1016/S0022-460X(88)80224-4.

[37] Hackbusch, W., 2012. Tensor spaces and numerical tensor calculus. Springer, Berlin New York.

[38] Au, S.K., 2012a. Fast Bayesian ambient modal identification in the frequency domain, Part I: Posterior most probable value. Mechanical Systems and Signal Processing 26, 60–75. doi:10.1016/j.ymssp.2011.06.017.

[39] Au, S.K., 2012b. Fast Bayesian ambient modal identification in the frequency domain, Part II: Posterior uncertainty. Mechanical Systems and Signal Processing 26, 76–90. doi:10.1016/j.ymssp.2011.06.019.

[40] Reynders, E., Maes, K., Lombaert, G., De Roeck, G., 2016. Uncertainty quantification in operational modal analysis with stochastic subspace identification: Validation and applications. Mechanical Systems and Signal Processing 66-67, 13–30. doi:10.1016/j.ymssp.2015.04.018.

[41] Jeff Wu, C.F., Hamada, M.S., 2000. Experiments: Planning, Analysis, and Parameter Design Optimization. Wiley, New York.

[42] Box, G.E.P., Hunter, J.S., Hunter, W.G., 2005. Statistics for experimenters: Design, Innovation, and Discovery. Wiley-Interscience, Hoboken, N.J.

[43] Charlier, C.V.L., 1928. A new form of the frequency function. Meddelanden fran Lunds Astronomiska Observatorium Serie II 51, 3–28.

[44] Kasinos, S., Lombardo, M., Makris, N., Palmeri, A., 2020. Dynamic response analysis of nonlinear secondary oscillators to idealised seismic pulses. Earthquake Engineering and Structural Dynamics 49, 1473–1495. doi:10.1002/eqe.3313.

[45] Spiteri, P., 2020. Parallel asynchronous algorithms: a survey. Advances in Engineering Software 149, 102896. doi:https://doi.org/10.1016/j.advengsoft.2020.102896.

[46] Pellissetti, M., Ghanem, R., 2000. Iterative solution of systems of linear equations arising in the context of stochastic finite elements. Advances in Engineering Software 31, 607–616. doi:https://doi.org/10.1016/S0965-9978(00)00034-X.

[47] Stratonovich, R., 1964. Topics in the theory of random noise. Gordon and Breach, New York.

[48] Di Paola, M., Ricciardi, G., Vasta, M., 1995. A method for the probabilistic analysis of nonlinear systems. Probabilistic Engineering Mechanics 10, 1–10. doi:10.1016/0266-8920(95)91891-U.

[49] Wojtkiewicz, S., Spencer Jr., B., Bergman, L., 1996. On the cumulant-neglect closure method in stochastic dynamics. International Journal of Non-Linear Mechanics 31, 657–684. doi:10.1016/0020-7462(96)00029-7.

[50] Roberts, J., Spanos, P., 2003. Random vibration and statistical linearization. Dover.

[51] Blatman, G., 2009. Adaptive sparse polynomial chaos expansions for uncertainty propagation and sensitivity analysis. PhD thesis, Institut Francais de Mécanique Avancée et Université Blaise Pascal.

[52] Gerstner, T., Griebel, M., 1998. Numerical integration using sparse grids. Numerical Algorithms 18, 209–232.

[53] Efron, B., Hastie, T., Johnstone, I., Tibshirani, R., 2004. Least angle regression. Annals of Statistics 32, 407–499.

[54] Xu, Y., Zhang, W., 2001. Modal analysis and seismic response of steel frames with connection dampers. Engineering Structures 23, 385–396. doi:10.1016/S0141-0296(00)00062-6.

[55] Kawashima, S., Fujimoto, T., 1984. Vibration analysis of frames with semi-rigid connections. Computers & Structures 19, 85–92. doi:https://doi.org/10.1016/0045-7949(84)90206-2.

[56] Hadianfard, M., Razani, R., 2003. Effects of semi-rigid behavior of connections in the reliability of steel frames. Structural Safety 25, 123–138. doi:https://doi.org/10.1016/S0167-4730(02)00046-2.

[57] de Luca di Roseto, A., Palmeri, A., Gibb, A.G., 2018. Performance-based seismic design of steel structures accounting for fuzziness in their joint flexibility. Soil Dynamics and Earthquake Engineering 115, 799–814. doi:https://doi.org/10.1016/j.soildyn.2018.09.007.

[58] Sekulovic, M., Salatic, R., Nefovska, M., 2002. Dynamic analysis of steel frames with flexible connections. Computers & Structures 80, 935–955. doi:10.1016/S0045-7949(02)00058-5.

[59] Computers and Structures, 2007. Sap2000. Release 15.2.1 .

[60] Makris, N., Chang, S.P., 2000. Effect of viscous, viscoplastic and friction damping on the response of seismic isolated structures. Earthquake Engineering and Structural Dynamics 29, 85–107. doi:10.1002/(SICI)1096-9845(200001)29:1<85::AID-EQE902>3.0.CO;2-N.

[61] Palmeri, A., Makris, N., 2008. Response analysis of rigid structures rocking on viscoelastic foundation. Earthquake Engineering and Structural Dynamics 37, 1039–1063. doi:10.1002/eqe.800.

[62] The MathWorks, Inc., 2013. Matlab. Release 8.2 .

[63] Kasinos, S., Palmeri, A., Lombardo, M., 2019. Ancillary computational tools for the analysis of structural systems, in: 7th International Conference on Computational Methods in Structural Dynamics and Earthquake Engineering.

[64] Fryba, L., 1999. Vibration of solids and structures under moving loads. Thomas Telford, London.

[65] Muscolino, G., Palmeri, A., Sofi, A., 2009. Absolute versus relative formulations of the moving oscillator problem. International Journal of Solids and Structures 46, 1085–1094. doi:10.1016/j.ijsolstr.2008.10.019.